Nanoscale

REVIEW

Nanodiamonds for field emission: state of the art

Maria Letizia Terranova,[a] Silvia Orlanducci,[a] Marco Rossi[b] and Emanuela Tamburri*[a]

Cite this: *Nanoscale*, 2015, **7**, 5094

Received 4th December 2014,
Accepted 28th January 2015

DOI: 10.1039/c4nr07171a

www.rsc.org/nanoscale

The aim of this review is to highlight the recent advances and the main remaining challenges related to the issue of electron field emission (FE) from nanodiamonds. The roadmap for FE vacuum microelectronic devices envisages that nanodiamonds could become very important in a short time. The intrinsic properties of the nanodiamond materials indeed meet many of the requirements of cutting-edge technologies and further benefits can be obtained by tailored improvements of processing methodologies. The current strategies used to modulate the morphological and structural features of diamond to produce highly performing emitting systems are reported and discussed. The focus is on the current understanding of the FE process from nanodiamond-based materials and on the major concepts used to improve their performance. A short survey of non-conventional microsized cold cathodes based on nanodiamonds is also reported.

Introduction

Miniaturized electron sources based on the field emission (FE) process, namely "cold-cathodes", are nowadays replacing the conventional thermoionic electron sources. FE-based devices are able to operate at high frequency and at high current densities, have no need of heating and are characterized by reduced weight and by instantaneous switching on. Moreover,

[a]*Dip.to di Scienze & Tecnologie Chimiche – MinimaLab, Università di Roma "Tor Vergata", Via Della Ricerca Scientifica, 00133 Rome, Italy. E-mail: Emanuela.Tamburri@uniroma2.it*

[b]*Dip.to di Scienze di Base e Applicate per l'Ingegneria & Centro di Ricerca per le Nanotecnologie applicate all'Ingegneria (CNIS), Università degli Studi di Roma "Sapienza", Via A. Scarpa, 00161 Rome, Italy*

Maria Letizia Terranova

Professor of Chemistry at Tor Vergata University of Rome (Italy), Maria Letizia Terranova heads the Minima lab at the Department of Chemical Science and Technology. She has expertise on different scientific topics, including nuclear chemistry, laser-induced reactions in the gas-phase, ion- and laser-induced modifications in solids, electrochemical and vapour deposition processes. Her research activity is mainly focused on the synthesis, processing and functional testing of nanomaterials: carbon nanostructures (nanodiamonds, nanotubes, graphenes, onions), nanocomposites and hybrid organic/inorganic structures. Materials and systems are produced for applications in micro/nano-electronics, optoelectronics, energetics, sensing, thermal management and bio-related nanotechnologies. She has co-authored 290 papers, 4 patents, and co-edited 4 books.

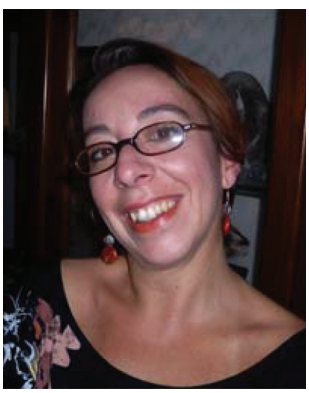

Silvia Orlanducci

In 2004 Silvia Orlanducci received her PhD in Chemical Sciences. Since 2007 she has been a Researcher at the Faculty of Science of the Tor Vergata University of Rome (Italy). Her research activity, performed in the frame of Inorganic Chemistry and Material Chemistry, is focused on the settling of synthesis methodologies, treatments and structural/functional characterizations of materials. Her main research line deals with carbon-based nanomaterials: nanodiamonds, nanotubes, and nanographites. She is a co-author of 129 papers published in peer-reviewed journals, the co-editor of 2 books and 2 patents.

the good performances of such devices are further greatly improved by using nanostructured materials as emitters.

Everything started in 1968, when Spindt, on the basis of the Fowler and Nordheim studies, explaining field emission as a quantum effect,[1] fabricated the first flat display using arrays of Mo microsized cones.[2] The theoretical research work by Fowler–Nordheim and the experiments by Spindt and co-workers[3] paved the way for a number of subsequent researches on FE-based vacuum electronics. The good performance of such devices is based on the fact that, according to the Fowler–Nordheim law, the emitted current density J depends strongly on the local applied electric field E and that geometric factors typical of nanostructures (sharp edges, tips, peaks, nanoprotrusions) locally increase the concentration of electric field at the emitter sites. The ratio of the local field to the applied field, the so-called electric field enhancement factor β,[1] independently of the material, is a key factor influencing the field emission characteristics.

In the last two decades the design, realization and application of a new generation of cold cathodes based on advanced nanomaterials have been the object of tremendous interest by researchers active in all the areas related to electron emission, from space applications to experiments in the field of high-energy physics. The aim has been to find materials and systems characterized by the best FE performances in terms of low turn-on field (corresponding to an electron emission density of 0.01 mA cm^{-2}), high density of the emitted current at low applied field, robustness and long-term stability of the emission.

Among the materials most extensively investigated, carbon nanotubes (CNTs) undoubtedly have a prominent place, due to their emission features and foreseen applications in advanced electronic devices.[4,5] In this regard, many efforts have been directed toward the issues of increasing the stability of the CNT field emission while decreasing the applied driving voltage. Many and different technological routes have been considered and studied. The most successful approaches proposed for the generation of promising starting blocks for vacuum electronic systems have been the embedding of nanotubes in a non-conductive polymer matrix[6] and the coating of CNTs with wide band gap materials (WBGMs).[7,8] One must consider that both non-conductive matrices and WBGM coatings are able to reduce the effective work function of the CNTs and the turn-on field for electron emission. Moreover, WBGM coatings are expected to act as a mechanical protection for the sharp conductive emitters.

In such a framework, the use of diamond as a CNT coating to stabilize the emission has attracted the interest and attention of many research groups.[9–20] All of these studies have reported enhancements of the emitting features and an increase of the CNT lifetime due to the diamond coverage; they have also evidenced the greater potential of diamond compared with other WBGMs. This could be hardly considered an unexpected result, because among the other WBGMs, diamond is characterized by very favorable properties, such as a high dielectric constant, a negative electron affinity (NEA), high thermal conductivity, mechanical strength, chemical inertness and radiation tolerance.[21–25] Moreover, the fact that the diamond surfaces do not adsorb chemical species has made it possible to use the emitters without the need for "conditioning" pre-treatments, consisting of complex out-gassing steps, as required in the case of uncoated CNTs.[26]

Let us consider in some detail the electronic structure of diamond. Cubic diamond (*e.g. Fd3m*) is a semiconductor with an indirect band gap of 5.5 eV. The valence band is fully occupied, the conduction band is empty. The bare surface of diamond has an electron affinity of +0.37 eV, while

Marco Rossi

As Professor of Physics at Sapienza University of Rome (Italy), Marco Rossi coordinates the Electron Microscopies and Nanoscopies Laboratory (EMINA) at the Department of Basic and Applied Sciences for Engineering. He is a member of the Scientific Board of the Centre of Research for Nanotechnologies applied to Engineering of Sapienza University of Rome (CNIS). His research activity is primarily aimed at the investigation of structural, functional and morphological features of C-based nanomaterials and their possible applications, using scanning probe and electron microscopies, X-Ray and electron diffraction techniques. He is a co-author of 160 papers and 1 patent, the co-editor of 1 book and 10 volumes of Proceedings.

Emanuela Tamburri

Emanuela Tamburri received a Laurea degree in Chemistry from the Sapienza University of Rome (Italy) in 2003, and a PhD in Chemical Sciences from Tor Vergata University of Rome (Italy) in 2008. She is currently a Post-doctoral Researcher at the Department of Chemical Sciences and Technologies and works as ab adjunct professor for the degree programs in Material Science. Her research interests include the synthesis and characterization of hybrid organic–inorganic composites and carbon-based nanostructures for electronic and optoelectronics, electrochemical sensors, gas sensors, and energy-related applications. She is a co-author of 91 papers and 1 patent.

the hydrogenated surface can reach NEA values down to about −3 eV.[21,27] Thus, the valence band of bare diamond is found at 5.9 eV, and that of H-terminated diamond at 4.2 eV below the vacuum level. The presence of the NEA in diamond also influences the work function, *i.e.* the energy difference between the Fermi and vacuum levels, producing a modulation of work function values that are similar to those of graphite and other C materials (about 5 eV).

A decrease of the diamond grain size below about 6 nm produces an increase of the band gap, due to quantum confinement effects. The size dependence of the band gap has been experimentally investigated by Bolker *et al.*[28]

Regarding the charge transport properties needed for electron emission, even if the diamond phase is intrinsically highly insulating, since the beginning of the "CVD diamond era" many synthetic approaches that are able to modulate and tailor the conducting or semiconducting behavior of diamond have been settled. As an example, it has been reported that p-type or n-type conductivities could be deliberately achieved by *in situ* B or N doping during the chemical vapor deposition (CVD) growth of diamond.[29–31] Semiconductive or metallic behavior can be also achieved through the use of oxides or metallorganic compounds during the growth.[32,33] It is well known that the doping procedures introduce defects and graphitic inclusions in the diamond lattice, but in any case the CVD processes themselves provide the co-deposition of an sp^2 conducting phase. Also, the post-synthesis procedures performed using plasma or ion beams act by inducing local phase transformation of the diamond to graphite or non-diamond carbons.[34,35] This is an important issue to be taken into consideration, because the inclusion of sp^2 graphitic patches has a strong effect on the mechanism of electron field emission from diamond. The presence of sp^2 phases is in particular of fundamental importance to rationalize the good field emission properties of nanodiamonds[28] that are characterized by a larger band gap with respect to bulk diamond, and would therefore be considered unattractive regarding the emission processes. The graphitic inclusions in nanodiamond deposits have a work function close to that of graphite (4.7 eV) and an energy about 1.4 eV above the valence band edge. It has indeed been demonstrated[36–42] that the non-diamond carbon content is the key factor for allowing easy electron conduction from the back to the front surface before the emission, which preferentially occurs from sharp tips or edges of diamond nanograins. In Fig. 1,[43] the scheme of a commonly accepted mechanism of emission from a coupled sp^2/sp^3 system is presented.

In this context, not only the shape and size of the nanocrystalline diamonds but also the phase composition play a role.

It is to be noted that the pioneering work by Wisitsora *et al.*[44] on the emission from diamond micro-tips had already evidenced the effects produced on cathode performances, not only by the shaping of the diamond emitters but also by the sp^2 content. These authors were the first to suggest a mechanism of field emission that was strongly correlated to the sp^2 content of the diamond.

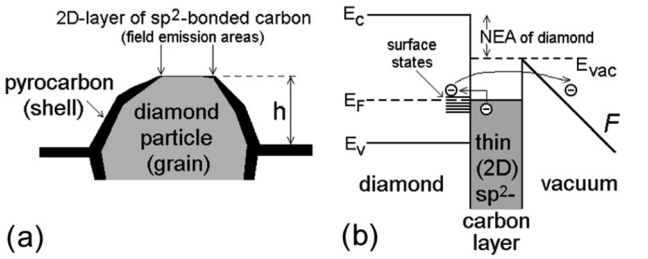

Fig. 1 Illustrations for a field electron emission mechanism from a coupled sp^2/sp^3 system. (a) Schematic surface structure of a diamond particle covered with a pyrocarbon shell; (b) emission from the diamond surface covered with a thin graphitic layer where electrons are injected from graphite to diamond and then emit as 'diamond electrons' through the barrier, lowered due to the NEA or band bending. Reprinted with permission from ref. 43; © 2001, Elsevier.

The emitting features shown by nanodiamond coupled with CNTs have created the demand for a deeper understanding of the capabilities offered by nanostructured diamonds as an effective player for the fabrication of "all diamond" cold cathodes. Opportunities to exploit knowledge gained from previous investigations on the emissions from nanodiamond and related systems come especially from the rapid progress in new application areas and from the need to overcome some technological bottlenecks that other materials cannot solve, as, for example, the thermal degradation of nanotubes during emission or the effects of adsorbates on the surface of the emitters. These drawbacks, of relative importance when cold cathodes are applied in many conventional electronic devices, are expected to become strongly limiting factors in the cases of less usual and most sophisticated applications. Based on the unique radiation and temperature tolerance of diamond, such electron sources can indeed work in plasmas, in high ion or neutron fluxes and in general in extreme environments, nowadays finding use in space-related applications, in nuclear reactor instrumentation and also in the driving of accelerators and free electron lasers (FELs).

This review aims to summarize existing research, to disclose new findings and to provide a roadmap for future developments in the area of diamond-based electron field emitters. The methodologies proposed since 2000 for the production of nanosized diamond systems suitable for the assembling of cold cathodes are surveyed and discussed. A short analysis of the emitting features obtained by using various diamond nanostructures is also given.

For the sake of clarity, the paper is organized with the following main sections: (1) nanodiamond films; (2) shaped diamond 1D structures; (3) detonation nanodiamond; and (4) nanodiamond-based devices.

Nanodiamond films

The first synthetic routes proposed for the fabrication of emitting diamond films were based on chemical vapor deposition (CVD) techniques, still widely employed for the preparation of nanocrystalline layers that can be easily integrated in Si circuit

technology. In view of the fact that the morphology and structure of the films depend strongly on the composition of the feeding gas, a variety of gas mixtures has been used to modulate the characteristics of the carbon deposits in terms of crystallinity and phase purity. A review reporting on the CVD growth of nanodiamond films has been published in ref. 45.

A specific class of nanodiamond films is the so-called ultrananocrystalline diamond (UNCD), firstly produced at the Argonne National Laboratory[46–48] using hydrogen-poor plasma chemistry. The inert gases (N_2, Ar, He, ...) added to the feeding gas phase play an important role by accelerating the high secondary nucleation rates, and the control of the H_2/noble gas ratio enables the production of nanocrystalline films with a grain size in the 2–5 nm range. The group headed by Gruen further optimized the deposition methodology, using mainly N for the doping and obtaining films with a high degree of conformality and very exciting FE properties.[49–55] Deep analysis of the films, performed by means of complex scanning probe microscopy methods, has evidenced in such films periodic structures where diamond crystallites are associated to high-conducting inclusions. Atomic force microscopy (AFM) in Spreading Resistance Imaging (SRI) configuration has allowed maps of the conductivity along the film nanostructure to be obtained. As a general rule, conduction in UNCD occurs at the grain boundaries, where the incorporation of N produces graphitic nanoregions. The images reported in Fig. 2 evidence the distribution of the highly conductive inclusions, corresponding to the nanoregions where emission occurs at the lowest field values.

A series of experiments have been designed and carried out in laboratories around the world to study the relationship between the FE features and some fundamental parameters, such as the sp^3/sp^2 ratio, the grain size and shape, the doping level, and the patterning. The low dimensionality of the grains and the shaping in elongated 1D structures have been found definitely to represent the key parameters for significant emission from diamond films. However, a critical analysis of the data indicates that several other aspects play a role.

Regarding the topic of doping, many papers have analyzed in detail the effects produced by adding nitrogen to the gaseous mixtures used for the synthesis of diamond nanostructures and their emission efficiency.[56–60] A general conclusion that can be drawn from the above reported studies is that the nitrogen incorporation into diamond not only induces an n-type conductivity, but also provides the formation of sp^2 hybridized carbon, which plays a fundamental role in FE from carbon nanostructures.[40] The insertion of nitrogen in the diamond lattice is generally achieved by adding N_2 to the gaseous feeding mixtures used for CVD-based growth, but in some cases different nitrogen sources have also been used. As an example, nitrogen doping was obtained in ref. 58 by using urea (NH_2CONH_2) in powder form, carried by gas fluxes and delivered to the active area of the deposition chamber by a tubing system. The use of urea as a reactant has been proved to generate a larger amount of nitrogen-vacancy defects with respect to those induced by the use of N_2. Such defects are claimed as very effective for the generation of a donor band in the diamond state,[61] and the coupling of this donor band with the conductive sp^2 channels leads to the enhancement of the emission properties.

In other experiments, the addition of He was found to produce layers with structures varying from nanocrystalline diamond with graphitic patches connecting the grains, to porous interconnected graphene networks.[62,63] Fig. 3 shows the various morphologies obtained by using He concentrations of 10, 20, 30 and 40%, respectively.

A methodology based on plasma-aided chemical deposition from CH_4–H_2–N_2 mixtures activated by a DC discharge has been reported in ref. 64. A series of nitrogen-containing nanodiamond films lacking any significant difference in phase composition and morphology were produced. Conversely, marked differences (up to 200×) were found when comparing the values of the emitted current from the various samples. This occurrence has been ascribed to needle-like carbon nanofibers present on the surface of the films that are produced at higher temperatures. In Fig. 4 is reported an impressive image showing the marked differences in the density of the emitting centers for samples grown at 950 and at 1030 °C.[64]

Nano-graphite filaments were found to play a role in the emission process also by Cheng *et al.*[65] while they were

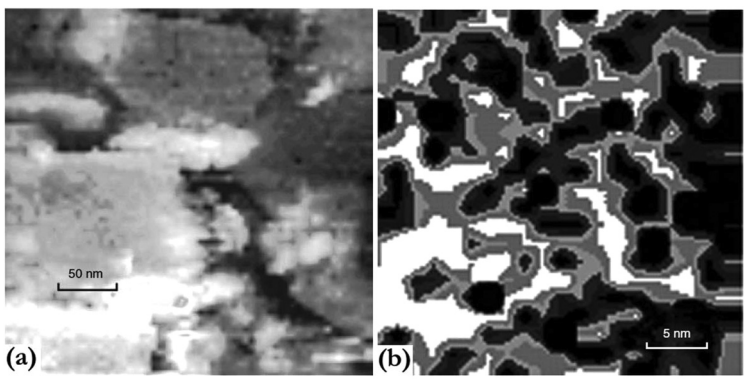

Fig. 2 Samples grown with 10% N_2 in the plasmas: (a) AFM-SRI map (320 nm × 320 nm); (b) AFM-SRI map (25 nm × 25 nm) showing the distribution of the film electroconductivity inside conglomerates. Reprinted with permission from ref. 50; © 2004, John Wiley & Sons, Inc.

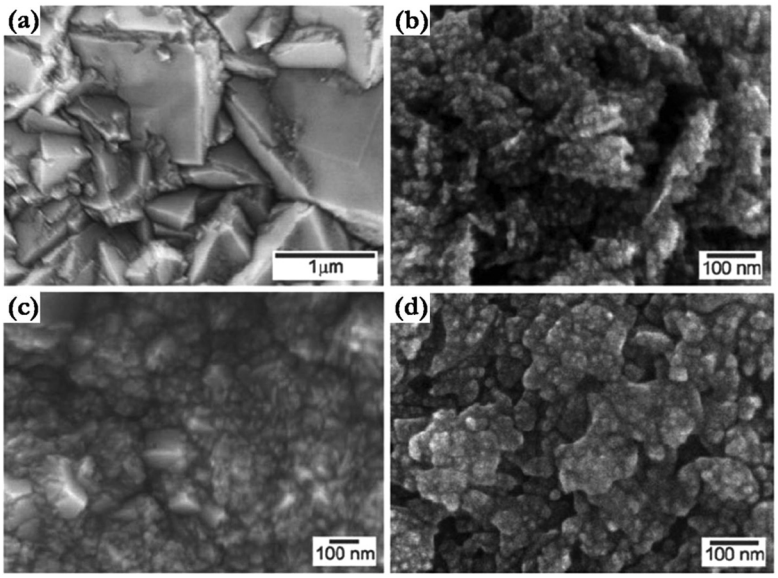

Fig. 3 Typical 'top-view' FESEM images of the samples after deposition for 3 h at different helium concentrations in the gas feed: (a) 10 vol%, (b) 20 vol%, (c) 30 vol%, and (d) 40 vol%. Reprinted with permission from ref. 63; © 2004, IOP Publishing.

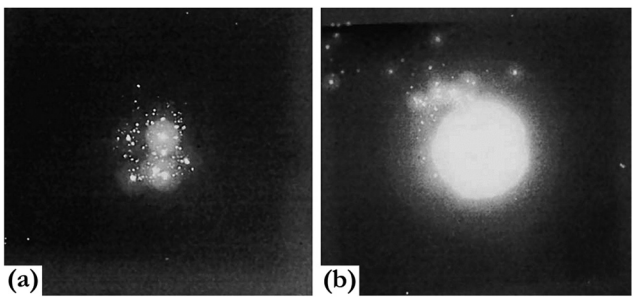

Fig. 4 Photographs of the screen (imaged area: 20 mm × 20 mm) showing the distribution of the FE centers on the cathode surface for samples prepared with a substrate temperature of: (a) 950 °C; (b) 1030 °C, respectively. Reprinted with permission from ref. 64; © 2009, Springer.

investigating the FE characteristics of diamond films produced by two different approaches, namely bias-enhanced-nucleation and bias-enhanced-growth processes. Their investigations enabled them to establish the plasma conditions for the production of films with a turn-on field as low as 3.6 V μm^{-1} and able to emit current densities up to 325 $\mu A\ cm^{-2}$ at an applied field of 13.5 V μm^{-1}. The good FE performances have been rationalized on the basis of the unique structure of the nanocrystalline diamond deposits (grain size: 10–30 nm) that were found to contain a large proportion of SiC particulates, likely produced by plasma-induced ion bombardment of the Si substrate. The growth of the SiC nanoparticulates was accompanied by that of nano-graphite filaments, around 5 nm in thickness and several tens of nanometers in length. The presence of such a nanographitic phase, extending all over the diamond film, greatly facilitates the electron transport through the film and is considered the key factor for improving the FE performances of these films with respect to those grown from conventional CH_4/Ar plasmas.

An approach based on properly bias-enhanced CH_4/Ar plasmas was found to greatly accelerate the nucleation and growth processes, producing through 10-min runs UNCD films with thicknesses of up to 380 nm.[66] The employed synthesis methodology induced the formation of graphitic nanoregions distributed inside the diamond film and at the interface, forming a network of conductive paths that facilitate the electron transport and the field emission process. The nanostructured films were used to assemble high-performance cold cathodes.

High current emissions were obtained from thin diamond films deposited using an innovative MW plasma-assisted CVD reactor adding both Ar and N_2 to CH_4–H_2 mixtures. Current densities of up to 220 A cm^{-2} were emitted under 50 ns high-voltage pulses with amplitudes of up to 100 kV. These highly efficient cathodes were successfully tested in a high-power pulsed RF compressor triggered by an electron beam.[67]

In the search for methodologies able to increase the conductivity and enhance the FE, some research groups have explored the strategy of metal-ion implantation in nitrogen-doped ultrananocrystalline diamond films. By implantation of Au and Cu ions in diamond films grown at rather low temperatures (T < 475 °C), Sankaran *et al.* produced free-standing, highly conducting films with emitted currents of up to 3.76 mA cm^{-2} at an applied field of 12.5 V μm^{-1}.[68] Afterwards, diamond films characterized by a conductivity up to a value of 185 $\Omega^{-1}\ cm^{-1}$, a low turn-on field (4.88 V μm^{-1}) and by a current density of 6.52 mA cm^{-2} at an applied field of 8.0 V μm^{-1} were produced by Au implantation.[69] The TEM image in Fig. 5 shows the dispersion of Au nanoclusters at the film/substrate interfaces. The outstanding emission features have been ascribed to the Au-induced formation of nanographitic

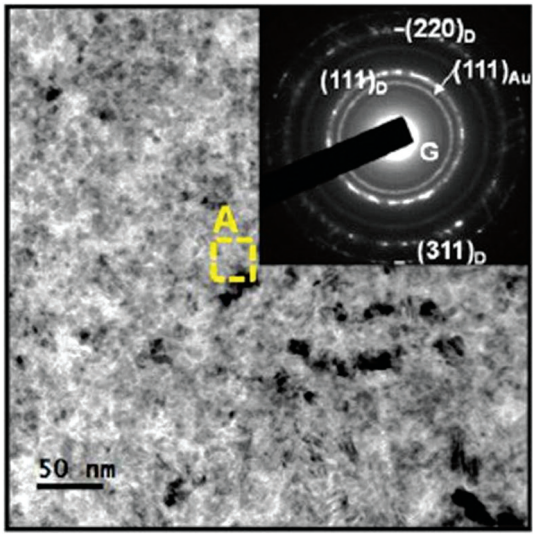

Fig. 5 TEM image of Au nanoclusters at the film/substrate interfaces with corresponding SAED pattern shown as inset. The spotted diffraction pattern arranged in the ring indicates the nanosized nature of the diamond and the gold phases. Reprinted with permission from ref. 69; © 2013, American Institute of Physics.

patches at the grain boundaries of the polycrystalline films, and to the opening of effective conducting channels for electron transport. A slightly reduced improvement in both the electrical conductivity and electron emission was instead obtained when Cu-ions were implanted in the same type of ultrananocrystalline diamond layers. From these films, current densities of up to 3.60 mA cm^{-2} at an applied field of 8.0 V μm^{-1} were measured.[70]

Interesting FE properties, with a turn-on field of 1.98 V μm^{-1} and a current density of 705 $\mu A\ cm^{-2}$ at 7.5 V μm^{-1}, were revealed in the case of nitrogen-containing UNCD films that were Fe-coated and post-annealed at 900 °C in a H_2 atmosphere.[71] These films were characterized by a unique granular structure formed by diamond grains (sizes <5 nm) and a uniformly distributed dense population of Fe nanoparticles, produced from the H-induced annealing of the Fe coating. The morphological features of the Fe nanodeposits can be observed in Fig. 6, which shows the stereographic projection and the *X*–*Y* projection of the TEM 3D-tomography. The process of Fe clustering induced, in turn, the formation of graphitic nanoregions surrounding the nanoparticles. The preferential emission of electrons from the graphitic regions was demonstrated by performing current imaging tunneling spectroscopy (CITS), which showed enhancement of the FE from the boundaries of the Fe nanoparticles.

A comprehensive investigation into the relationship between the structure of the implanted UNCD films and the emission behavior has been carried out in ref. 72. In both the Au- and Cu-implanted layers the SEM investigation evidenced pronounced morphological changes induced by the ion implantation, with modifications from an equi-axed granular structure, typical of pristine UNCD films, into a featureless

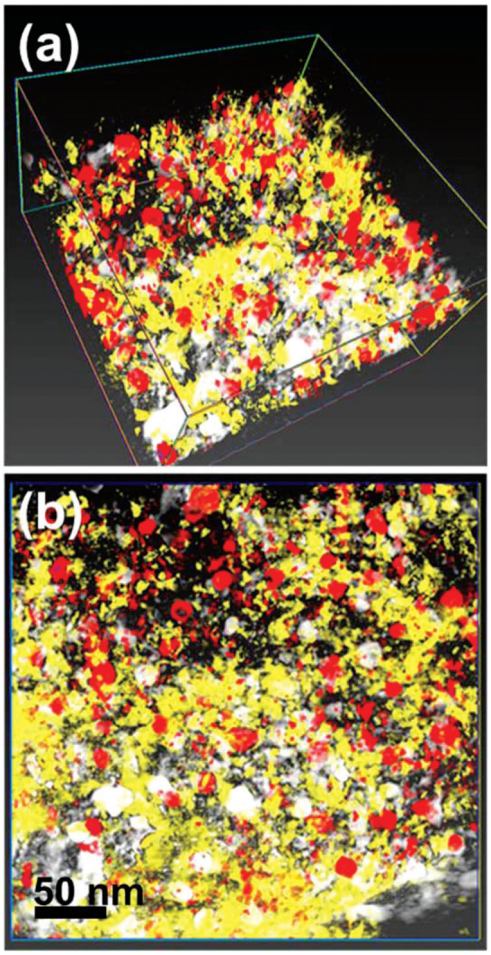

Fig. 6 (a) Stereographic projection and (b) *X*–*Y* projection of the TEM 3D-tomography of an $(Fe/UNCD)_{900}$ film. Reprinted with permission from ref. 71; © 2013. AIP Publishing.

morphology.[72] In Fig. 7 the field emission curves of the pristine UNCD, of the Cu-UNCD, and of the Au-UNCD films are reported along with the corresponding Fowler–Nordheim (F–N) plots.

The mechanism behind the enhanced FE properties of both the Au- and Cu-implanted UNCD films has been rationalized taking into account the results of the structural characterizations, which showed that, in all of the samples, the formation of metallic nanoclusters was homogeneously distributed within the films. However, differences were found in the shape of the Au and Cu nanoclusters. Whereas implanted Au ions were found to form spherically shaped Au nanoparticles, HRTEM investigations revealed plate-like Cu nanoparticles arranged in row-like patterns. The morphological features of the Au and Cu clusters were found to modulate the proportion of nanographitic phases at the grain boundaries of the nanodiamond film. Rather larger amounts of nanographitic phases were detected at the Au-nanodiamond grain boundaries with respect to those surrounding the Cu clusters, and this finding can explain the better emission performance exhibited by the Au-implanted diamond films.

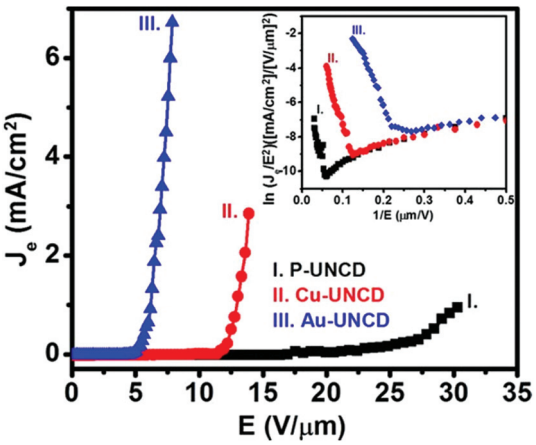

Fig. 7 Electron field emission properties (J_e–E curves) of: (I) pristine UNCD; (II) Cu-UNCD; (III) Au-UNCD films. The inset shows the corresponding F–N plots. Reprinted with permission from ref. 72; © 2014, American Chemical Society.

The role of the graphitic phases surrounding the diamond nanocrystallites in improving the emission has been directly confirmed by CITS. Fig. 8, taken from ref. 72, shows the local electron emission behavior and evidences that electrons are prevalently emitted from the grain boundaries.

1D structures

Starting from the systematic investigations of Wisitsora *et al.*[44] it has been demonstrated that the FE from nanodiamond films could be strongly enhanced by shaping the diamond in the form of elongated low-dimensional structures, such as nano-rods, nano-wires, nano-tips, nano-whiskers and nano-pillars. The energetic stability, theoretical aspects and preferable morphology of the diamond 1D nanostructures have been deeply investigated by Barnard in ref. 73.

The increase of the emission properties in sharpened diamond has been commonly ascribed to the formation of tips and to the related increase of the field enhancement factor β.[74] The idea underlying such an interpretation is that the lines of the applied field concentrate at the tips, lowering the barrier for electron emission. However, the nanometric control of diamond materials into the desired and tailored geometries, as those required for fabrication of cold cathodes, is really a challenging and complex task.

1D-shaped nanodiamond systems have been and still are fabricated by several methods, including top-down lithographical approaches,[75,76] bottom-up growth using CVD with templates,[77] plasma-aided CVD growth without spatial confinement,[25,78,79] and plasma post-synthesis treatments.

Among the various methodologies proposed for shaping the diamond into pointed structures, the most successful and more widely used are based on the plasma treatments of plane diamond films. Using such approaches it is possible to produce both polycrystalline and single-crystal 1D structures, with diameters spanning several tens of nanometers.

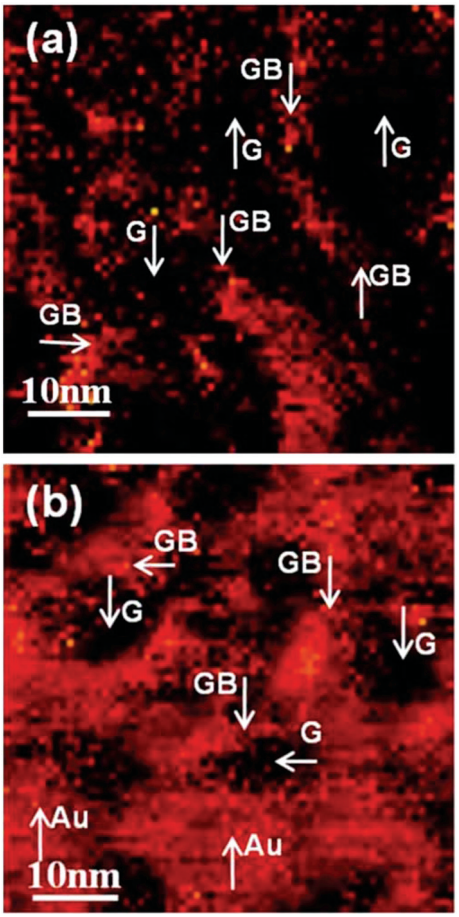

Fig. 8 CITS image of (a) Cu-UNCD, and (b) Au-UNCD films. The typical grains and grain boundaries are marked as "G" and "GB", respectively. Reprinted with permission from ref. 72; © 2014, American Chemical Society.

There are many options for the plasma etching of materials. The shaping of diamonds in pointed structures that able to offer a high emission efficiency can be successfully performed using plasmas generated by different sources, such as radio-frequency (RF), microwave (MW), direct current (DC), electron cyclotron resonance (ECR), inductively coupled plasma (ICP), neutral loop discharge (NLD).[80–83] In some cases, plasmas produced by the coupling of two different sources are used. All these sources are capable of delivering high-density plasmas and can provide an efficient and reliable way to fabricate diamond-based micro- and nano-structures.

The first studies on the etching of diamond were performed on high pressure–high temperature (HP/HT) single-crystal samples using an O_2/H_2 RF plasma.[84] Starting in 1990, several studies have addressed the use of a suitable gas or of gas mixtures to realize plasma treatments of single-crystal or polycrystalline diamond flat plates,[34,85] obtaining nanowire arrays with or without applying a mask. These findings have opened the way for the design and fabrication of pointed diamond nanostructures also for emitting purposes.

By using a mask and a CH_4/O_2 RF plasma Ando *et al.*[86] produced high-quality single-crystal diamond nanorods on a (100)

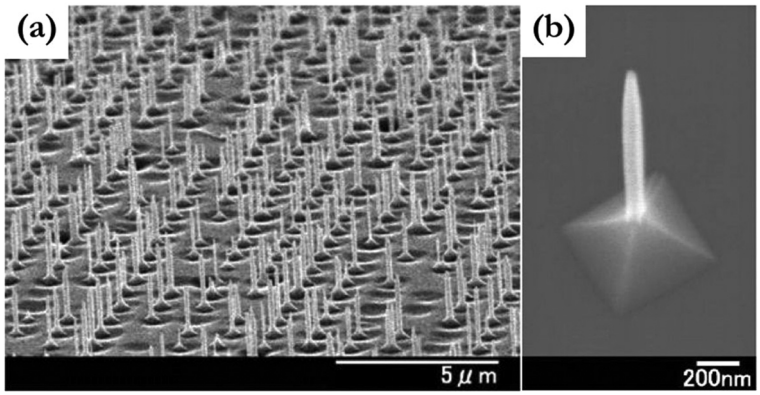

Fig. 9 SEM micrographs of H-plasma treated HP/HT synthetic diamond with a (100) surface: (a) an array of diamond nano-rods; (b) an isolated nano-rod. Reprinted with permission from ref. 86; © 2004, Elsevier.

oriented diamond crystal. Fig. 9 shows SEM images of an array of diamond nanorods and details of a single crystalline nanorod.

Aligned diamond nanowires were obtained by Smirnov *et al.*[87] using self-aligned Ni nanoparticles as a mask and carrying out the etching using an oxygen inductively coupled plasma.

The combination of a strongly anisotropic O_2/CHF_3 plasma etching with a hexagonally patterned nanomask made by Au nanoparticles was the approach used in ref. 88 to produce the densely packed arrays of diamond nanotips shown in Fig. 10. The emission was found to be greatly enhanced with respect to the emission from untreated, pristine B-doped diamond films.

An upsurge of publications related to mask-free processes for the fabrication of very efficient diamond emitting systems has occurred over the last few years.

A forest of straight diamond rods longer than 6 μm have been fabricated by etching a polycrystalline diamond film in an O_2 RF plasma reactor.[89] Each of the shaped rods was found to be formed by two conical single crystalline diamond grains. Ref. 76 illustrates a modified bottom-up electron beam lithography/reactive ion etching (EBL/RIE) method based on the selective seeding RIE process which enables the growth of horizontally aligned ultrananocrystalline nanowires (width about 90 nm) at pre-defined positions on the substrate. The scheme of the process is shown in Fig. 11.

A series of uniform and high-density nanostructures have been selectively engineered from diamond films characterized by a variety of granular morphologies.[90] Cone-shaped and tip-shaped nanostructures were obtained from microcrystalline diamond using a CF_4/O_2 plasma; conversely, pillar-like and grass-like forms were obtained from nitrogen-doped ultrananocrystalline diamond using an Ar plasma. The authors thoroughly investigated the relationship between the structure/morphology of the nano-shaped deposits and important functional properties such as photoluminescence and electron emission. In Fig. 12 can be observed the different morphologies of the nanostructures, obtained by RIE etching of microcrystalline films (a), from nanocrystalline films (b), from

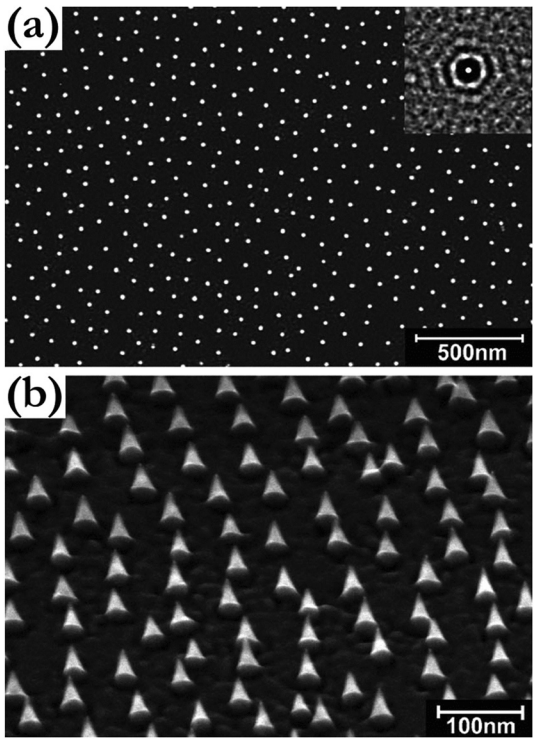

Fig. 10 SEM pictures of a diamond surface nanostructured by combining self-assembled micellar Au nanomasks with anisotropic reactive ion etching: (a) top view; (b) sample tilted by 50° relative to the surface normal. The inset of (a) gives the lateral correlation function indicating a high degree of hexagonal order. Reprinted with permission from ref. 88; © 2006, Elsevier.

ultrananocrystalline films (d), and from nitrogen-doped ultrananocrystalline films (e). The corresponding FE curves are also reported (c,f). It is evident that the most appealing FE properties are exhibited by the nanosized diamond forms originating from UNCD.

Hydrogen plasmas have been and still are widely used to etch diamond films. As already evidenced in early studies on plasma-treated diamond,[35,91] the effect of the etching, which is

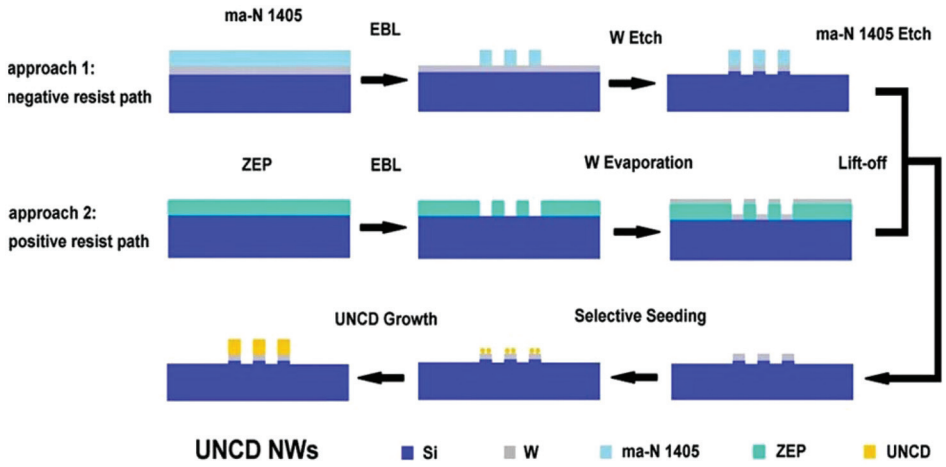

Fig. 11 Schematic of ultrananocrystalline diamond nanowire fabrication processes by a modified bottom-up EBL/RIE method based on selective seeding by both RIE and lift-off. Reprinted with permission from ref. 76; © 2012, IOP Publishing.

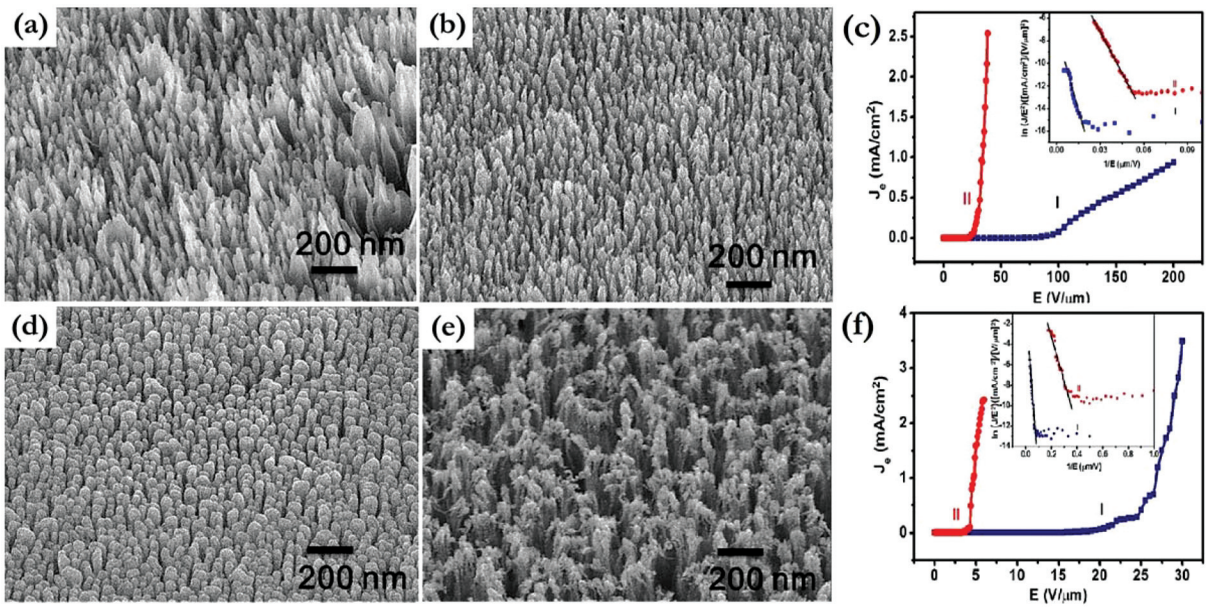

Fig. 12 FESEM micrographs of 30 min RIE etched nanostructures: (a) nanocones from microcrystalline films; (b) nanotips from nanocrystalline films; (d) nanopillars from ultrananocrystalline films; (e) nanograss from nitrogen-doped ultrananocrystalline films. The corresponding FE curves are also reported: (c) nanocones (curve I) and nanotips (curve II); (f) nanopillars (curve I) and nanograss (curve II). Reprinted with permission from ref. 90; © 2013, American Chemical Society.

dependent on the orientation of the diamond nanocrystallites, is enhanced when a negative DC bias is applied. The mechanism acting in the formation of sharpened diamond structures by negative-biased plasmas is briefly schematized in the following. The hydrogen ions generated by the plasmas, regardless of the plasma source is, are accelerated by the electrical field and compelled to stream downward to the sample surface. The electrons emitted from the diamond film produce a modification in the plasma configuration. The resulting inhomogeneous distribution of the electrical field lines induces a more intense ion impact at the grain boundaries, where sp^2 nanodomains or defective sp^3 clusters are confined. The resulting effect is a preferential etching of the grain boundary zones and a subsequent growth of vertically elongated nanostructures. Depending on the plasma conditions, and specifically on the kinetic energies of the ions, a variety of columnar nanoshaped diamond deposits can be obtained. A schematic diagram that illustrates the etching process induced by a H_2/Ar plasma under negative bias has been proposed by Zou *et al.*[92] The scheme depicted in Fig. 13, in its general lines, can be considered valid also for plasmas generated by other gases.

The treatments in H-plasmas not only act by shaping flat diamond plates, but can be also viewed as a feasible solution for hydrogenating the diamond surface, modifying and

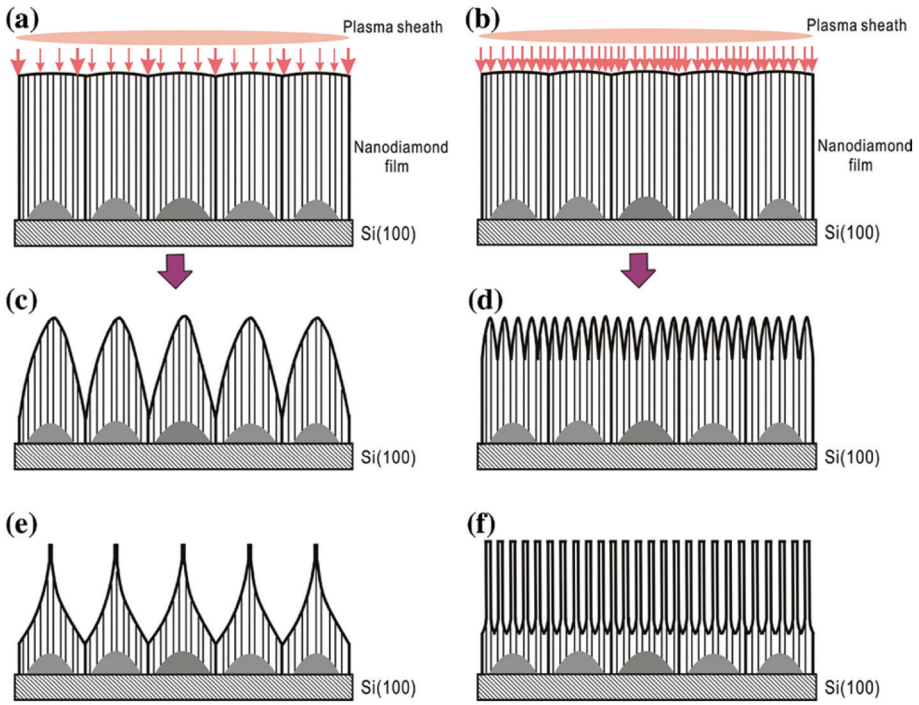

Fig. 13 Schematic representation of the bias-assisted RIE process on polycrystalline diamond films. The inhomogeneous distribution of the electrical field causes a preferential impact of the ions at the boundaries, as denoted by the arrows in (a) and (b) for the low and high ion kinetic energies, respectively. As a result, different surface morphologies are structured under the RIE conditions of: (c) and (d) low and high ion kinetic energies, respectively, in H-plasmas; and (e) and (f) low and high ion kinetic energies, respectively, in H_2/Ar plasmas. Reprinted with permission from ref. 92; © 2007, Elsevier.

tailoring the intrinsic NEA of the diamond. A lowering of the electron emission barrier due to the hydrogen-terminated diamond surfaces induced by the H-etching has been measured in ref. 92–94. The investigation of the NEA in H-etched polycrystalline samples revealed that high electron intensities were emitted from defective sites or graphitic/amorphous phases confined in grain boundaries, confirming that the electric field was unevenly distributed over the diamond surface.[93,94]

The bias-assisted H-etching can provide nanocone arrays with high aspect ratios, sharp tips, and high uniformity in geometry and size over a large area. Fig. 14 shows the SEM image (Fig. 14a) of an array of diamond nanocones produced by plasma etching of nanosized grains[95] and the TEM image (Fig. 14b) detailing dimensions and single-crystalline nature of a single nanotip. As reported in ref. 95, the turn-on fields were 26.9, 6.2, 18.2, and 10.1 V μm^{-1} for the pristine flat nanocrystalline diamond film, a low-density nanocone array, a high-density nanocone array, and an array of single-crystal diamond nanocones, respectively. The significant reduction of the turn-on field by lowering the nanocone density from 10^8 cm^{-2} to 10^6 cm^{-2} is likely due to the elimination of the screening effect acting between adjacent emitters.

Sharp tips (of radius as small as 2 nm) are easily obtained by the action of energetic H ions impinging at a right angle on the negatively polarized substrate. The formation of nanocones

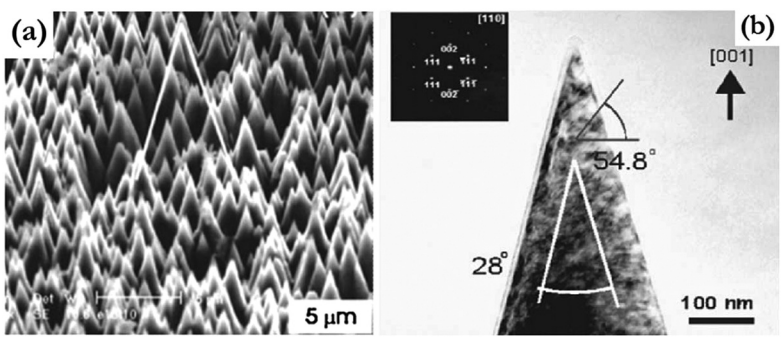

Fig. 14 (a) SEM images of a single-crystal diamond cone array; (b) TEM image of a diamond nanotip showing the sharp, single-crystal nature. The inset is the corresponding SAED pattern. Reprinted with permission from ref. 95; © 2003, AIP Publishing.

by H-etching occurs, as a general rule, through the following steps. The removal of the material starts from the grain boundaries, and the process proceeds by sharpening the isolated nanograins to obtain the final conical features as a consequence of an etching rate that is faster across the height of the gradually protruding diamond structures.[95–97]

A programmed treatment consisting of nitrogen plasma immersion ion implantation has been carried out on crystalline diamond nanotips (~1 μm in height, ~200 nm bottom diameter) produced by MW-enhanced CVD.[78] After the nitrogen treatment a turn-on field of 3 V μm^{-1} and a current density up to 4 mA cm^{-2} at the applied field of 9 V μm^{-1} were measured. HRTEM observations of the crystalline elongated objects evidenced nanosized amorphous regions, due to the disruption of sp^3-coordinated bonds and the subsequent creation of structural defects induced by the accelerated N-ions (Fig. 15).

On the basis of several similar results published around the same time, it has been suggested that the good emission exhibited by the sharpened diamond deposits could be ascribed to both the high aspect ratio geometry and to the electron-conducting pathway in the C-sp^2 layer.[98] This interpretation has opened a new scenario. Even if the protruding sharp structures certainly increase the field enhancement factor β,[1] by concentrating upon themselves the field lines, at that time there was only a small amount of evidence that electrons were emitted from such sharp tips. Wide confirmation was instead accumulated from the presence of graphitic phases. The surface of sharp structures generated by various techniques or plasma etching are always found to be coated by thin layers of amorphous carbon with a high sp^2 content. Recently, Panda *et al.*[99] produced diamond nanowires by H-plasma etching of nitrogen-containing diamond films generated by a MW-CVD process. The H-plasma treatments produced wire-like diamond nanocrystals encased in a nanographitic sheet (Fig. 16a) with turn-on fields of 4.2 V μm^{-1}, and current densities of up to 5.1 mA cm^{-2} at an applied field of 8.5 V μm^{-1}. The systematic investigation of the effect of H-etching on both the FE and conductivity (up to 216 Ω cm^{-1}) evidenced a strong enhancement of the emission properties produced by rather short H-plasma treatment times (<10 min). Conversely, a degradation of the same properties was found to occur for etching processes longer than 15 min, as one can see from the FE data shown in Fig. 16b. This has been ascribed to the removal, induced by prolonged H-etching, of the graphitic phase surrounding the diamond nanowires.[99]

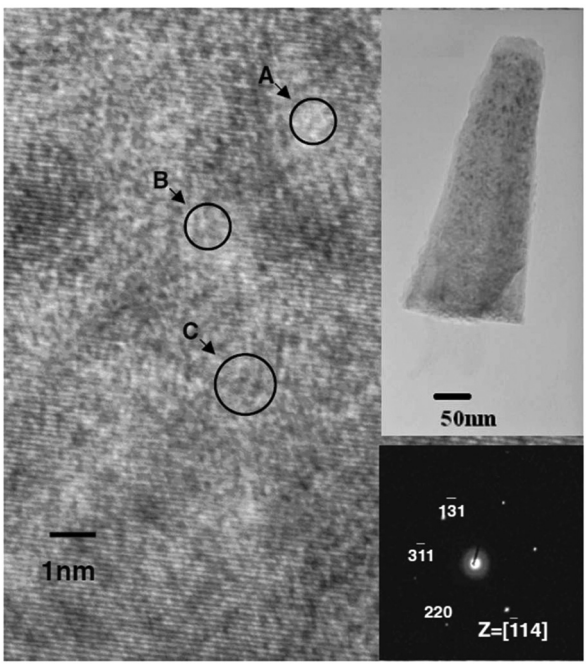

Fig. 15 HRTEM lattice image of a diamond nanotip treated with nitrogen plasma immersion ion implantation for 10 min. A clear lattice image with several nanoscale amorphous regions, circled and marked 'A', 'B' and 'C', is observed in a crystalline diamond crystal structure. The bright-field HRTEM image of the diamond nanotip is inserted in the upper-right corner. The electron diffraction pattern of the diamond nanotip is inserted in the lower-right corner. Reprinted with permission from ref. 78; © 2007, IOP Publishing.

A direct observation of the emitting sites in plasma-shaped diamond samples has recently been achieved by Chatterjee *et al.*[100] by employing scanning tunnel microscopy (STM) apparatus. The results reported in ref. 100 confirm the hypothesis that the emission occurs mainly from the non-diamond phases located at the grain boundaries between the pointed nanostructures.

Another suitable option to prepare cone-shaped diamond nanostructures is that of using the focused ion beam (FIB) technology. As reported in ref. 101 high aspect ratio nanocone arrays with controlled densities could be produced *via* FIB milling of a freestanding undoped diamond film characterized by a moderate sp^2 carbon content. The emission from the nanocone arrays reached 88 μA at 15 V μm^{-1}. Emission from the back surface of the same film only reached 10 μA at 15 V μm^{-1}. The authors estimated that the average emission current from an individual diamond cone with an apex radius of about 60 nm was around 13 nA. Under the assumption of electrons being emitted mainly from the hemispherical apex, the average current density per cone would be 5.8×10^4 mA cm^{-2}.

A study on the FE as a function of the inter-tip distance has been carried out in ref. 102. Fig. 17a–c shows the SEM images of nanotip arrays with inter-tip distances of 5, 10 and 20 μm. Fig. 17d shows the current intensity as a function of the applied field for the three different nanocone arrays and for the pristine planar film.

Further strategies that have been explored look at the incorporation of nanosized diamonds inside specifically configurated substrates. An example of such a fabrication approach is illustrated in ref. 103. Here, arrays of pyramidal shaped UNCD microtips, produced by depositing conductive nanodiamonds inside inverted pyramidal microcavities, have been applied on a plastic substrate. Fig. 18 illustrates the scheme of the fabrication process.

Fig. 19 shows a typical array of inverted pyramidal microcavities homogeneously coated by nanodiamond. For arrays of

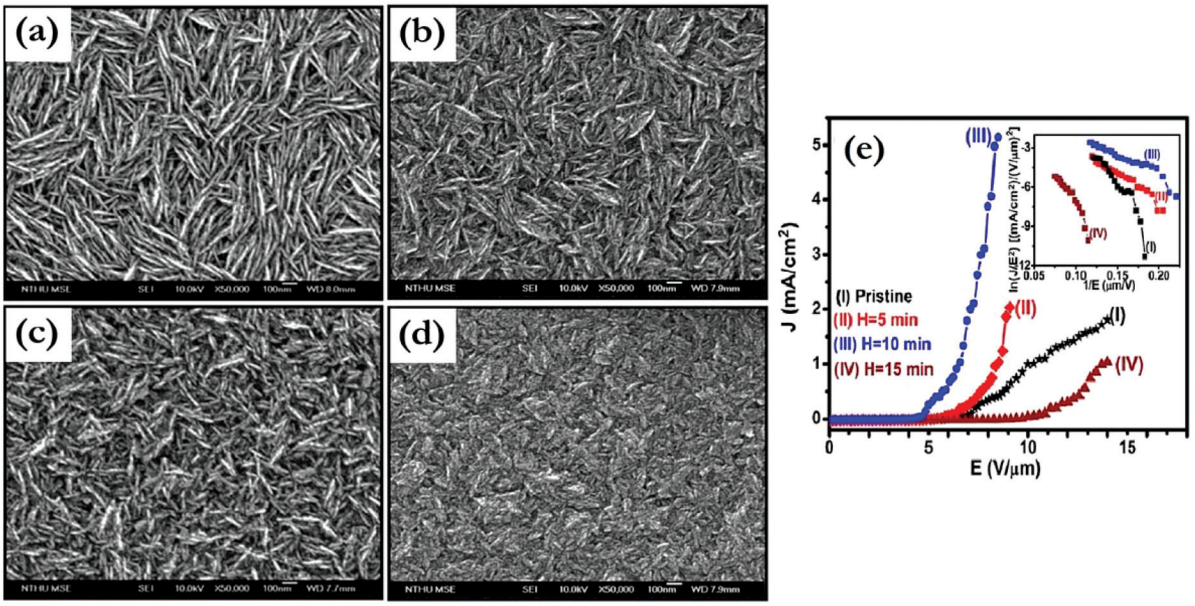

Fig. 16 FESEM images of: (a) pristine and (b–d) H-plasma-treated diamond nanowires for: (b) 5, (c) 10; and (d) 15 min. The field emission current density (*J*) as a function of applied electric field (*E*) is reported in (e) for: (I) pristine; (II) 5 min; (III) 10 min; and (IV) 15 min H-plasma-treated films. The inset presents the corresponding F–N plots. Reprinted with permission from ref. 99; © 2014, American Chemical Society.

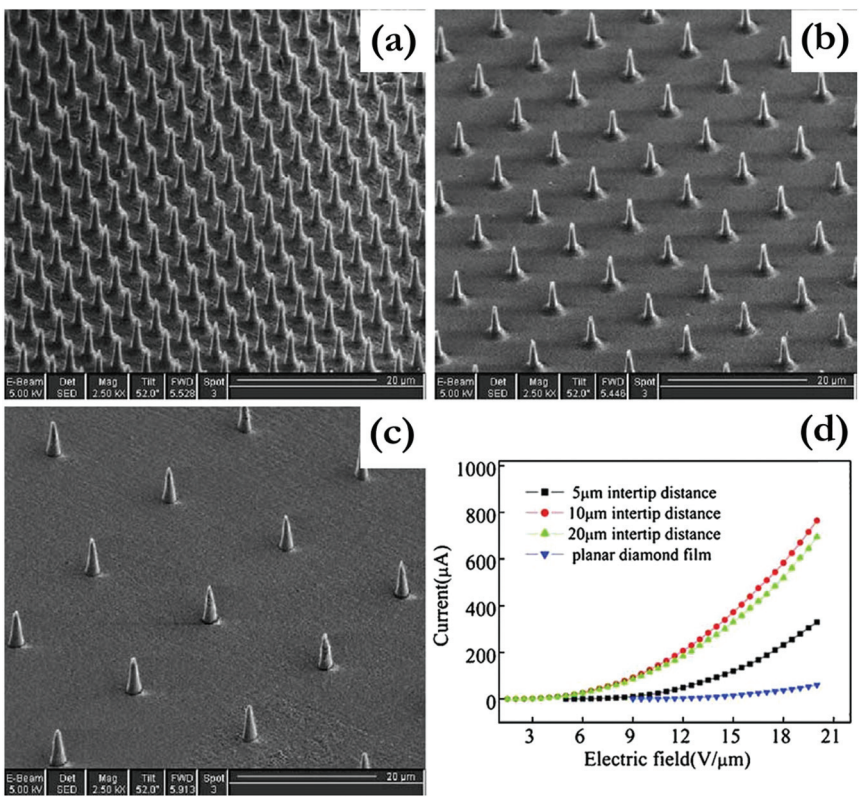

Fig. 17 SEM images of high aspect ratio conical diamond tip arrays on the freestanding diamond film. The corresponding inter-tip distances are: 5 μm (a), 10 μm (b), 20 μm (c), respectively. (d) The (*I*–*E*) curves of field emission from the conical diamond tip arrays with different inter-distances and that from the planar diamond film. Reprinted with permission from ref. 102; © 2006, Elsevier.

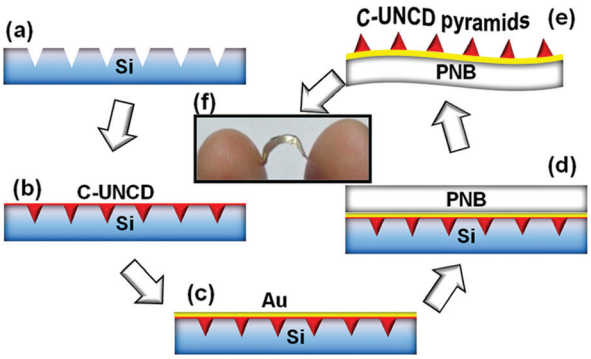

Fig. 18 Schematic of the process for fabricating flexible, conducting-UNCD (C-UNCD) pyramidal microtips: (a) anisotropic etching of the Si substrates using a potassium hydroxide–*n*-propanol–deionized water solution to form inverted pyramidal microcavities; (b) deposition of C-UNCD films on the inverted pyramidal microcavities using the MW plasma CVD system; (c) sputtered deposition of Cr (5 nm) and Au (100 nm) on the C-UNCD films; (d) spin coating of polynorbornene (PNB); (e) arrays of flexible C-UNCD pyramidal microtips after etching of Si; (f) digital photograph of typical, hand-bent, flexible C-UNCD pyramidal microtips. Reprinted with permission from ref. 103; © 2014, AIP Publishing.

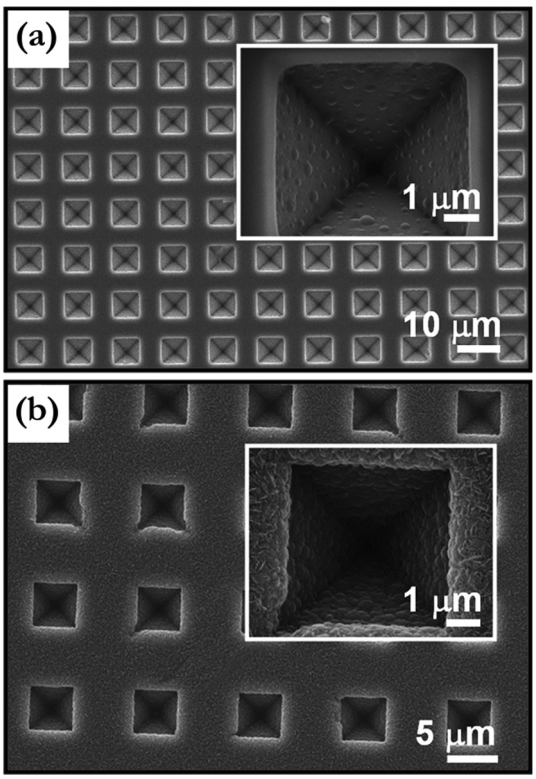

Fig. 19 FESEM image of: (a) typical arrays of inverted pyramidal microcavities created on the Si substrate, with the inset showing a magnified image of a single inverted pyramidal microcavity; and (b) the C-UNCD-film-coated inverted Si pyramidal microcavities, with the inset showing the a magnified image of a C-UNCD-film-coated single inverted pyramidal microcavity. Reprinted with permission from ref. 103; © 2014, AIP Publishing.

2 μm tips, a turn-on field of 1.80 V μm^{-1} and a current density of 5.8 mA cm^{-2} at an applied field of 4.20 V μm^{-1} have been measured.[103] Flexible devices based on the diamond pyramidal microtips open a prospect for a new generation of flat panel displays and high brightness electron sources.

Plasma-assisted CVD growth has proved to be a viable approach to produce, without the use of a mask, ensembles of sharpened diamond that are formed directly during the synthesis step. In ref. 79, diamond nanocone arrays were produced using CH_4–H_2 mixtures in a bias-enhanced dual-mode RF-MW plasma reactor under well-controlled conditions. The H-ion bombardment led to localized conversion of the growing diamond into graphitic or amorphous phases, which were further chemically etched by the activated hydrogen species in the plasma. The conical-shaped structures are the result of an interplay between the competing growth and etching processes.

Detonation nanodiamond

In the context of nanodiamond materials employed to assemble cold cathodes, a specific mention must be given to the so-called "detonation nanodiamond".[104] In this case the nanodiamond, in powder form, is extracted from the soot produced by a detonation process. The first published papers on detonation nanodiamond[105,106] immediately evidenced the attractiveness of this member of the crystalline carbon family have and inspired researchers to perform investigations that also look at the emission properties. With respect to the electron emission, detonation nanodiamond indeed shows some advantages over CVD-generated and/or plasma-etched nanodiamond deposits.[107]

One must consider that nanodiamonds are polyhedral objects (crystallites with sizes in the 4–6 nm range), with distinct faceting. It has been reported how the polyhedral shape affects the stability of the surface of small particles, including the graphitization of the surface to form fullerenic bubbles. This instability gives rise to an sp^3 core surrounded by an external shell of sp^2 carbon. HRTEM images (taken from ref. 104) of typical detonation soot, purified nanodiamond and oxidized nanodiamonds are shown in Fig. 20. The diamond peak of the purified (blue line) and oxidized (red lines) nanodiamonds can be seen at 1328 cm^{-1} in the Raman spectra. A further important aspect of this kind of nanodiamond is the presence of surface electrostatic potential, which changes with particle size and induces the formation of agglomerates with a preferred particle/particle orientation and drives the assembly of nanodiamond with other chemical species.[108–112] A sketch of the normalized surface electrostatic potential for relaxed structures of cuboctahedral-shaped nanodiamonds is displayed in the inset in Fig. 20. The sketch has been illustrated in ref. 108, where a deep discussion on the physical properties of the nanodiamond surfaces can also be found.

The intrinsic core/shell architecture of detonation nanodiamonds converts into a practical form the concept of the sp^2/sp^3 mixture that was definitely found to govern field emission from carbon nanostructures. Moreover, differently from the as-produced CVD films, the nanosized polyhedral crystals of deto-

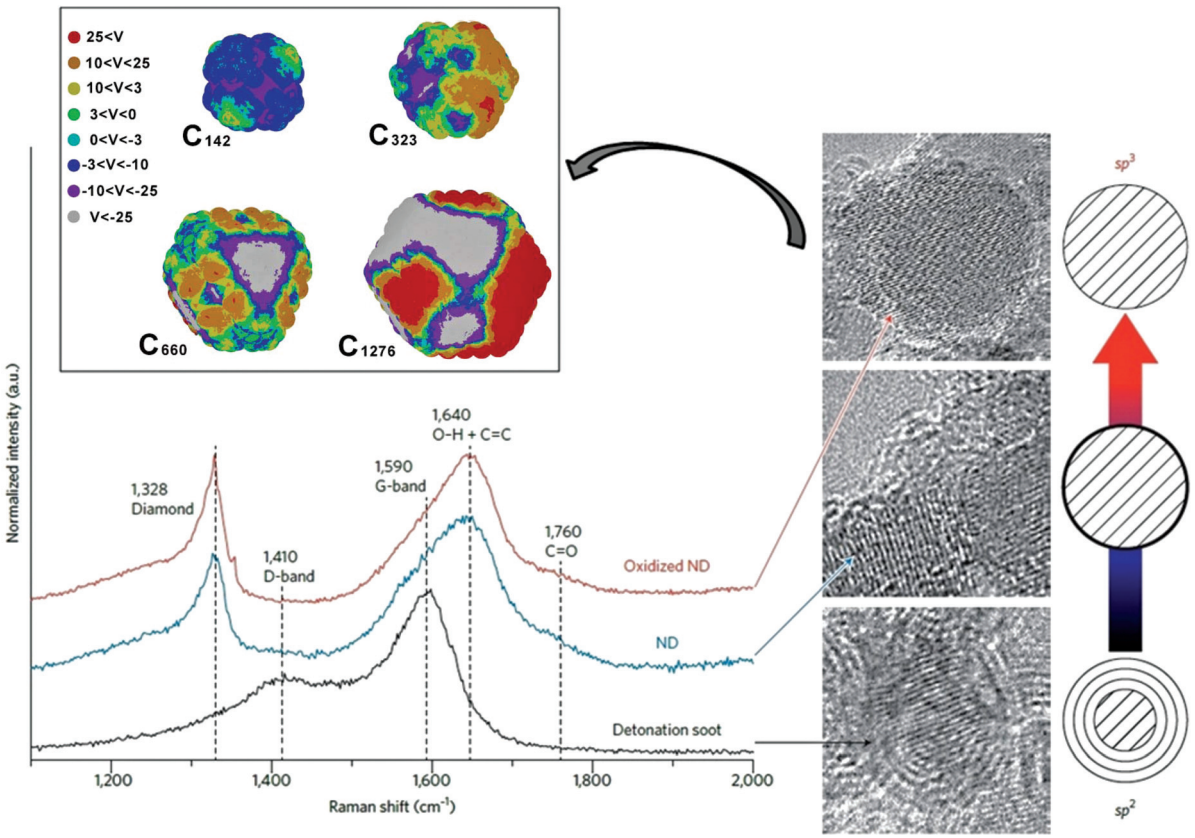

Fig. 20 Electron micrographs showing detonation soot (bottom), purified nanodiamond (middle) and oxidized nanodiamond (top). The diamond cores in the purified nanodiamonds are partially covered by a thin layer of graphite that allows observation of the diamond peak at 1328 cm^{-1} in the Raman spectrum (blue line). In the inset the normalized surface electrostatic potential for relaxed structures of cuboctahedral-shaped nanoparticles is shown. Adapted and reprinted with permission from ref. 104 (© 2012, Nature Publishing Group) and 108 (© 2007, Royal Society of Chemistry).

nation diamond offer spontaneously a large number of sharp edges, eliminating the need for etching treatments.[111]

The first results on the use of detonation nanodiamond as a cold emitter material were presented in dedicated conferences and have received widespread publication in books.[113–115] After the first intense phase of investigations had established the emitting features of this exciting new nanomaterial, detonation nanodiamond can now be considered a rather "mature" emitting material, upon which activities of applied research for cathode prototyping and technological transfer have been carried out.[112]

Nanodiamond-based devices

Effective downscaling and microintegration of emitting systems, coupled with substantial advances in novel cold cathode geometries, are offering brilliant solutions for a variety of rapidly evolving technologies.

Nowadays, vacuum integrated circuits based on nanodiamonds have been proposed by several research groups. Hsu *et al.*[116] fabricated a vacuum field emission transistor (VFET) based on nitrogen-incorporated nanodiamonds. The diamond phase was deposited by CVD on cavities patterned on silicon oxide insulating (SOI) substrates, and the microfabrication technique that was used enabled the achievement of gate-controlled emission currents and good signal amplification. The alternating current (AC) voltage gain resulted in agreement with the theoretical model.

In ref. 117 a basic circuit building block consisting of an integrated differential amplifier is described in detail. This device is based on an array of vertically configured nanodiamond emitters integrated with partition gates and split anodes. The dual-mask fabrication procedure involved the steps of nitrogen-doped nanodiamond deposition into micropatterned molds on SOI substrates and the mold-transfer, followed by partitioning of the Si gate and the formation of individual nanodiamond FETs. The SEM image of two adjacent nanodiamond-based VFETs is shown in Fig. 21 along with the image of a vertically configured cathode and details of the emitting surface. The inset of Fig. 21b evidences a single emitter cathode with an ultrasharp apex. Such nitrogen-incorporating ultrasharp diamond emitters have been produced by plasma-enhanced CVD from CH_4–H_2–N_2 mixtures. The device fabricated following the procedure reported in ref. 114 matched well the characteristics of a VFET, with a low gate turn-on voltage and negligible gate intercept current.

Nanodiamond can be also used to fabricate notable non-contact RF transducers.[118] Current densities up to 500 nA per nanodiamond tip at an applied bias of 30 V have been

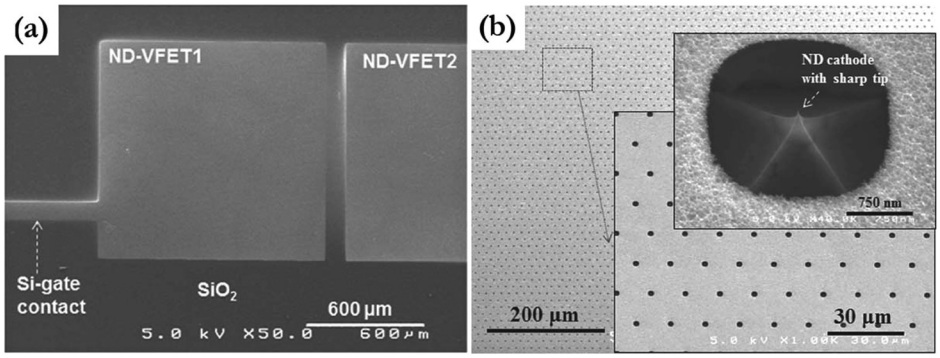

Fig. 21 FESEM images of: (a) a pair of nanodiamond vacuum field emission transistors (ND-VFETs) (top-viewed); and (b) part of an ND-VFET with insets showing a higher magnification and a single ND cathode with self-aligned Si gate. Reprinted with permission from ref. 117; © 2013, IEEE.

achieved by processing B-doped 200-nm-thick layers. In ref. 118 an innovative design is described that, through the choice of a suitable chip architecture and the engineering of the material, allowed the realization of a low-barrier electron emitter and of an RF piezo-actuator in the same microsized device.

The concept of FE from nanodiamond has been also proposed for engineering flat panel X-ray sources.[119] The cathode prototype consisted of an FE array of N-containing ultrananocrystalline deposits, fabricated using conventional microfabrication techniques. A current density of about 6 mA cm^{-2} at an applied field of 10 V μm^{-1} has been produced. The experimental data were compared with the output of simulations in order to define alternative gate configurations and to assure a beam of highly collimated electrons. Such flat-panel X-ray sources are being tested for medical and industrial imaging applications.

The material properties, device structure and fabrication process are different aspects to be taken into consideration when dealing with the fabrication of this final generation of cold cathodes. Several alternative concepts of nanodiamond-derived vacuum emitters have recently been proposed and tested in order to realize devices with high speed, low power dissipation, robustness and long working life. An advantageous configuration is that of the planar lateral emission, firstly developed at the Diamond Laboratory of Vanderbilt University.[120] As illustrated in ref. 121 and 122, nitrogen-doped diamond films with a grain size of 5–10 nm, obtained by $CH_4/H_2/N_2$ MW plasma-enhanced CVD on SOI substrates, were patterned by RIE to fabricate a lateral FE diode device equipped with six fingers (inter-electrode separation: 3 µm). The lateral diode exhibits a turn-on field of 1.9 V μm^{-1}, and a high emission current of 1.1 mA (~183 µA current per finger) at an applied field of ~30 V μm^{-1}. The emission current was found to be stable over 10 h with ~4% fluctuation. Using the same process and by varying the electrode geometry, a series of lateral diodes, triodes and transistors were thereafter fabricated.[120,121] A 6-finger nanodiamond lateral field emission diode[123] is shown in Fig. 22. The vacuum-packaged device produced a current of over 3 µA at about 10 V μm^{-1} applied field, and exhibited a linear F–N plot. The operating characteristics

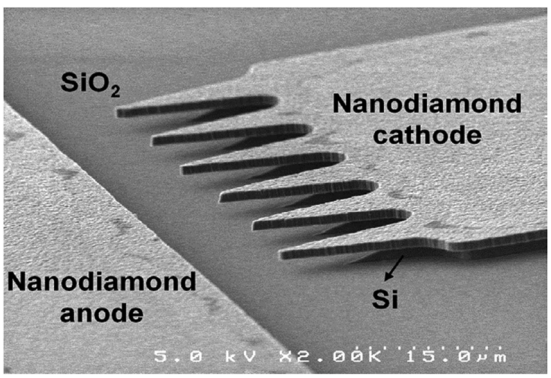

Fig. 22 SEM picture of a "6-finger" lateral nanodiamond vacuum emission diode (2000×). Reprinted with permission from ref. 123; © 2011, Elsevier.

of monolithic vacuum devices fabricated through applying such technology were not affected by X-ray irradiations of up to 20 Mrad or high fluences of up 4×10^{13} neutrons cm^{-2}.[123]

Frontier researches are nowadays focused on the design of a variety of vacuum field emission micro- and nano-devices with novel configurations, such as lateral emitting diodes, triodes, transistors and integrated amplifiers.[124] Some examples of nanodiamond-based lateral field emission devices can be viewed in Fig. 23.

Logic gates represent a further exciting envisaged application of the field emission from diamond.[125] Patterning highly-conductive 1-µm-thick films (5–10 nm grain size) by a pure O_2 plasma using an Al mask allowed researchers to define the lateral cathode and anode structures of vacuum microelectronic OR logic gates.[126] It has been demonstrated that the input/output logic values and the OR response can be optimized by increasing the emission area and the number of emission sites in the fingered structures.

Also in another outstanding technological area, namely that of accelerators and free electron lasers, the technology of nanodiamond emitters comes to play an attractive role. The characteristics of FE in RF fields have been reviewed by Li *et al.*[127] The aim of this research was to demonstrate the feasibility of using field emitter arrays and planar emitters based on

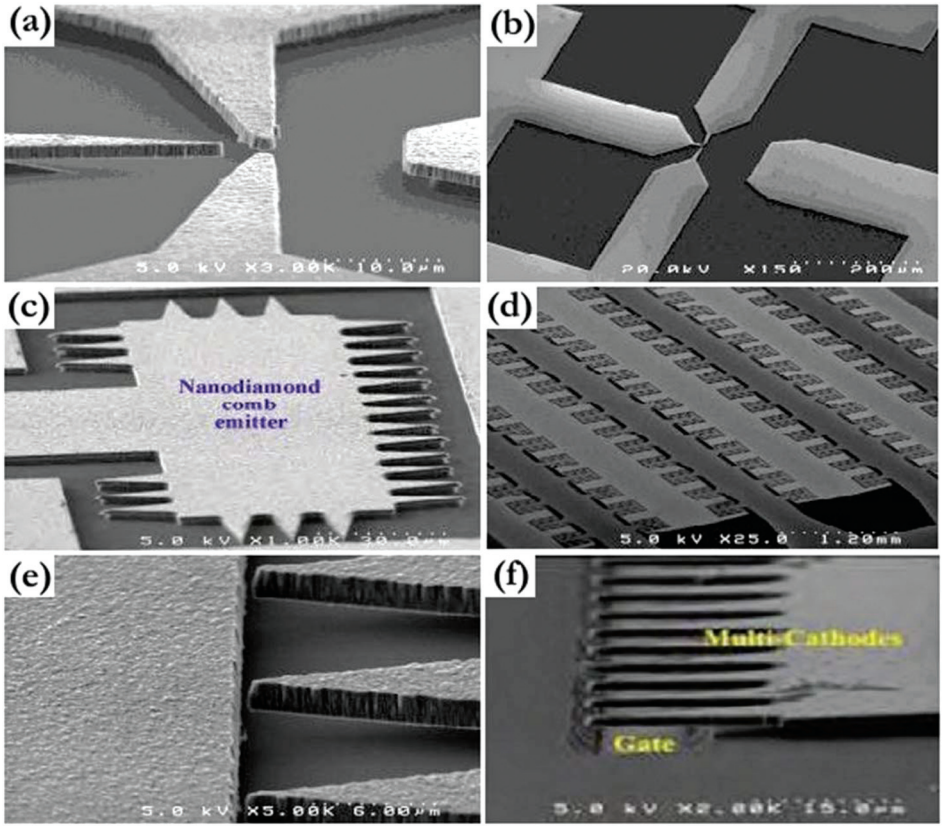

Fig. 23 Examples of nanodiamond vacuum lateral devices. SEM images of: (a) triodes; (b) transistors; (c) comb diode arrays; (d) large integrated diode arrays; (e) nano-gap diode arrays, and (f) common-gated triodes. Reprinted with permission from ref. 124; © 2012, IEEE.

diamond to drive accelerators and FELs. Experimental studies performed by installing a single cell test cavity have been compared with results obtained by simulations. The investigation indicated that low emittance and low energy spread bunches can be produced for amplitudes of the electric field on the cathode surface in the 60–90 MV m^{-1} range. Electric fields of up to 90 MV m^{-1} could be achieved when installing a half-cell S-band in the RF gun, making it possible to obtain high current electron bunches to drive a compact THz-FEL facility.

Conclusions

In the last decade, the class of nanodiamonds has been more and more investigated within the framework of research activities looking for efficient and robust emitting materials that also have the outstanding ability to work in hostile environments.

The unique advantages of nanodiamond and related materials place them at the forefront of the R&D activities related to cold cathodes, despite the fact that electron emission from diamond cannot reach the current densities measured for carbon nanotubes.

First of all, as for all the devices operating by the field emission mechanism, the nanodiamond-based cold cathodes show an almost instantaneous response to field variations. Moreover, due to its structural high stability, diamond can carry high current densities for long periods of time without any degradation. Additional benefits are chemical inertness and tolerance to high doses of radiation.

The present paper surveys the state-of-the-art of material design and procedures, putting in evidence those that are more promising for building highly efficient field emitting systems, for a wide collection of near-term and future technologies.

The various applications require not only the capability for generating nanodiamonds with specific intrinsic properties in terms of conductivity and of field emission, but also for retaining strong control over the organization of the nanostructures in predefined architectures. In this context, we attempted to illustrate the many exciting research challenges and technological opportunities related to the fabrication of cold cathodes based on nanodiamonds.

The first consideration is that the downsizing of the diamond grains is, in any case, able by itself to guarantee noticeable improvements of the field emission from the diamond. It is indeed well known that polycrystalline layers formed by microsized crystallites are characterized by very low densities of emitted current, also at rather high applied fields. Understanding the changes in the emission features as the grain dimensions decrease has been an important and widely pursued research issue, and the downscaling of diamond is

now considered the first focal goal to be reached by the use of suitable fabrication processes or post-synthesis procedures.

The next point concerns the shape of the emitters. The F–N law with its geometrical field enhancement factor β points out that, independently of the material, the emission is enhanced when the material is modeled in pointed shapes. The ratio between the height and the radius curvature of the tips governs the increase of emission from the tips with respect to that from plane deposits. All of the experimental data obtained to date conform to the F–N equation.

However, in the case of diamond, the roadmap for the fabrication of alternative efficient devices that are impervious to temperature and radiation needs much more than the features of downsizing and shaping in elongated nanostructures. In the process of preparing, characterizing and fabricating prototype devices using such nanomaterials, we have learned that the emission is driven by the sp^2 content of the diamond samples. Here we are at the heart of the concept of field emission from the diamond phase: a graphitic component is essential for obtaining reasonably good current densities. This is one of the rare cases in which, from phase purity, the functional properties of the materials do not derive benefits, but rather drawbacks. As a matter of fact, since the first experimental investigations performed in the 1990 s on the relationship between emission behavior and nanostructure, diamond that is characterized by high phase purity has been demonstrated to be a poor emitter. However, only recently, direct observations of the emission sites have allowed the role of graphitic phases in making diamond a suitable field emitter to be verified. Electron emission is now confirmed to occur preferentially from the sp^2-coordinated nanodomains that open very efficient conducting channels for electron transport and tunneling into diamond, even at low applied fields.

As regards the sp^2 content, its intentional or unintentional presence is in any case ascribable to the synthesis procedures. Optimization of the electron emission from diamond is nowadays pursued using methodologies that allow control over the structure at the nanoscale to be retained and to model both the content and location of the sp^2 inclusions. Among the most widely used synthesis approaches for producing low-dimensional diamond films, one can cite the growth of UNCD by plasma-assisted CVD from gaseous mixtures rich in inert gases. The small size of the diamond crystallites (2–5 nm) is the result of high secondary nucleation rates, promoted by the inert gases in a H-poor plasma. The presence of the sp^2 phase at the grain boundaries of the UNCD films can be rationalized by considering that, in a H-poor plasma, this phase cannot be etched away efficiently.

Various strategies, mainly based on plasma-enhanced CVD, have been suggested to produce films with grain sizes of >10 nm. The graphitic deposits surrounding the crystallites assured in any case good emission features and these nanomaterials are candidates for the assembly of highly performing cold cathodes.

Moving from such strategies towards a completely different approach, namely the implantation of metal ions into nanocrystalline diamond films, one discovers that the performances of these latter materials can be explained as well by a favorable combination of diamond and graphite phases. In effect, the ultimate result of Cu, Fe or Au implantation is the generation of, during the metal clustering process, dense populations of graphitic nanoregions along the grain boundaries. The enhancement of the FE properties may thus be viewed as a secondary effect of the ion implantation, and can be directly ascribed to the presence of nanographites.

A successful category of emitting nanodiamonds refers to the 1D structures that are currently produced by direct CVD techniques or by post-synthesis treatments using high-energy sources.

A large variety of techniques and of corresponding set-ups have been investigated, aiming at obtaining materials with increased emitting properties, and intensive research efforts are still being devoted to the engineering of emitters with designed features. One must consider, however, that the patterning of diamond in sharpened forms is always accompanied by the presence of sp^2 phases that are produced by the synthesis or post-synthesis techniques. This unavoidable graphitic component also plays a prominent role in the case of pointed emitters, and the control of the sp^2 inclusions is nowadays a fundamental issue pursued in several laboratories.

It is to be noted that the shaping of diamond in 1D nanostructures is also gaining quite an important place for other applications, such as DNA sensing,[128] bio- and electro-chemistry,[87] gas sensing[129] and quantum information.[130]

The final considerations regard the practical implementations of FE-based innovative devices that take advantage of the outstanding properties of nanodiamond. Analysis of the more recent literature evidences that, in the search for new ways to fabricate cold cathodes, synthesis processes, post-synthesis procedures and assembly methodologies are no longer independent issues to be faced individually, but rather are an entangled aspect of the same task. This approach is allowing the production of a new generation of non-conventional and highly performing vacuum field emission devices, with unlimited possibilities of use in areas related to space, nuclear reactors, and accelerators.

As regards space applications, the use of diamond-based cold cathodes is being considered not only for the substitution of conventional flat panel displays and other electron-beam vacuum devices sensitive to cosmic rays, but also for propellant ionization and ion beam neutralization in electrical propulsion systems. The technological demands of the space community are also leading to the testing of these robust and efficient electron emitters for the fabrication of on-board mounted devices, such as ionization sources for compact spacecraft mass spectrometers and for the fabrication of miniaturized X-ray tubes.

High-power pseudo-spark switches based on nanodiamond cathodes are tested as substitutes in Thyratrons or Spark Gaps in high-power excimer lasers and pulse power modulators in linear accelerators.

In the field of advanced vacuum microelectronics for communications, researchers are deeply exploring bipolar devices and monolithic lateral microtriodes that are characterized by a long working life that can also operate within high-temperature and harsh-radiation environments.

It is hoped that the results obtained so far could inspire further developments in the design of new nanodiamond-based architectures that could be converted into practical forms. The goal is to solve multisectorial technological issues, reducing the gap between research, industrialization and production.

List of acronyms

AC	Alternating current
AFM	Atomic force microscopy
CITS	Current imaging tunneling spectroscopy
CNT	Carbon nanotube
CVD	Chemical vapor deposition
DC	Direct current
EBL	Electron beam lithography
FE	Field emission
FEL	Free electron laser
FESEM	Field emission scanning electron microscopy
FET	Field emission transistor
FIB	Focused ion beam
HP/HT	High pressure–high temperature
HRSEM	High resolution scanning electron microscopy
HRTEM	High resolution transmission electron microscopy
MW	Microwave
NEA	Negative electron affinity
RF	Radio frequency
RIE	Reactive ion etching
SAED	Selected area electron diffraction
SEM	Scanning electron microscopy
SOI	Silicon on insulator
SRI	Spreading resistance imaging
STM	Scanning tunnel microscopy
TEM	Transmission electron microscopy
UNCD	Ultrananocrystalline diamond
VFET	Vacuum field emission transistor
WBGM	Wide band gap material

References

1 R. H. Fowler and L. W. Nordheim, *Proc. R. Soc. London, Ser. A*, 1928, **119**, 173.
2 C. A. Spindt, *J. Appl. Phys.*, 1968, **39**, 3504–3505.
3 I. Brodie and C. A. Spindt, *Adv. Electron. Electron Phys.*, 1992, **83**, 1.
4 W. A. de Heer, A. Chatelain and D. Ugarte, *Science*, 1995, **270**, 1179–1180.
5 K. B. K. Teo, E. Minoux, L. Hudanski, F. Peauger, J. P. Schnell, L. Gangloff, P. Legagneux, D. Dieumegard, G. A. J. Amaratunga and W. I. Milne, *Nature*, 2005, **437**, 968.
6 R. C. Smith, J. D. Carey, R. J. Murphy, W. J. Blau, J. N. Coleman and S. R. P. Silva, *Appl. Phys. Lett.*, 2005, **87**, 263105.
7 W. K. Yi, T. W. Jeong, S. G. Yu, J. N. Heo, J. H. Lee, W. Kim, J. Yoo and J. Kim, *Adv. Mater.*, 2002, **14**, 1464–1468.
8 K. Yu, Y. S. Zhang, F. Xu, Q. Li, Z. Q. Zhu and Q. Wan, *Appl. Phys. Lett.*, 2006, **88**, 153123.
9 M. L. Terranova, S. Orlanducci, A. Fiori, E. Tamburri, V. Sessa, M. Rossi and A. Barnard, *Chem. Mater.*, 2005, **17**, 3214–3220.
10 S. Orlanducci, E. Tamburri, M. L. Terranova and M. Rossi, *Chem. Vap. Deposition*, 2008, **14**, 241.
11 Fiori, S. Orlanducci, V. Sessa, E. Tamburri, F. Toschi, M. L. Terranova, A. Ciorba, M. Rossi, M. Lucci and A. S. Barnard, *J. Nanosci. Nanotechnol.*, 2008, **8**, 1989.
12 X. Xiao, J. W. Elam, S. Trasobares, O. Auciello and J. A. Carlisle, *Adv. Mater.*, 2008, **17**, 1496.
13 N. Shankar, N. G. Glumac, M. F. Yu and S. P. Vanka, *Diamond Relat. Mater.*, 2008, **17**, 79.
14 V. Guglielmotti, S. Chieppa, S. Orlanducci, E. Tamburri, F. Toschi, M. L. Terranova and M. Rossi, *Appl. Phys. Lett.*, 2009, **95**, 222113.
15 A. Vul', K. Reich, E. Eidelman, M. L. Terranova, A. Ciorba, S. Orlanducci, V. Sessa and M. Rossi, *Adv. Sci. Lett.*, 2010, **3**, 110–116.
16 Y. Zou, P. W. May, S. M. C. Vieria and N. A. Fox, *J. Appl. Phys.*, 2012, **112**, 044903.
17 K. J. Sankaran, K. Srinivasu, K. C. Leou, N. H. Tai and I. N. Lin, *Appl. Phys. Lett.*, 2013, **103**, 251601.
18 L. Yang, Q. Yang, C. Zhang and Y. S. Li, *Thin Solid Films*, 2013, **549**, 42–45.
19 D. Varshney, A. V. Sumant, O. Resto, F. Mendoza, K. P. Quintero, M. Ahmadi, B. R. Weiner and G. Morell, *Carbon*, 2013, **63**, 253–262.
20 T. Chang, S. Kunuku, K. J. Sankaran, K. C. Leou, N. Tai and I. N. Lin, *Appl. Phys. Lett.*, 2014, **104**, 223106.
21 F. J. Himpsel, J. A. Knapp, J. A. Van Vechten and D. E. Eastman, *Phys. Rev B: Condens. Matter*, 1979, **20**, 624.
22 S. Gildenblat and P. E. Schmidt, *"Diamond" Handbook series on Semiconductor Parameters*, ed. M. Levinstein, Singapore World Scientific, 1996, vol. 1, pp. 58–76.
23 O. Shenderova, D. Brenner and R. S. Ruoff, *Nano Lett.*, 2003, **3**, 805.
24 H. Watanabe, C. E. Nebel and S. Shikata, *Science*, 2009, **324**, 1425.
25 C. H. Hsu, S. G. Cloutier, S. Palefsky and J. Xu, *Nano Lett.*, 2010, **10**, 3272.
26 I. Boscolo, S. Cialdi, A. Fiori, S. Orlanducci, V. Sessa, M. L. Terranova, A. Ciorba and M. Rossi, *J. Vac. Sci. Technol.*, 2007, **25**, 1253–1258.
27 J. Robertson, *J. Vac. Sci. Technol., B*, 1999, **17**(2), 659–665.
28 A. Bolker, C. Saguy, M. Tordjman and R. Kalish, *Phys. Rev B: Condens. Matter*, 2013, **88**, 035442.
29 C. Wang, A. Garcia, D. C. Ingram and M. E. Kordesh, *Electron. Lett.*, 1991, **27**, 1459.

30 M. W. Geis, N. N. Efremov and J. D. Woodhouse, *IEEE Electron Device Lett.*, 1991, **12**, 456.
31 W. Zhu, P. Kochanski, S. Jin and L. Seibles, *J. Vac. Sci. Technol., B*, 1996, **14**(3), 2011–2019.
32 M. L. Terranova, V. Sessa, S. Piccirillo, M. Rossi, G. Micocci, A. Serra and A. Tepore, *Appl. Phys. Lett.*, 1999, **75**, 379–381.
33 A. Serra, D. Manno, T. Siciliano, G. Micocci, A. Tepore, M. Rossi, M. L. Terranova, V. Sessa, S. Piccirillo and S. Orlanducci, *J. Appl. Phys.*, 2003, **94**, 416–422.
34 A. Joshi and R. Nimmagadda, *J. Mater. Res.*, 1991, **6**, 1484.
35 B. R. Stoner, G. J. Tessmer and D. L. Dreifus, *Appl. Phys. Lett.*, 1993, **62**, 1803.
36 S. Bhattacharyya, O. Auciello, J. Birrel, J. A. Carlisle, L. A. Curtiss, A. N. Goyette, D. M. Gruen, A. R. Krauss, J. Schlueter, A. Sumant and P. Zapol, *Appl. Phys. Lett.*, 2001, **79**, 1441–1443.
37 F. A. M. Kõck, J. M. Garguilo and R. J. Nemanich, *Diamond Relat. Mater.*, 2014, **13**, 1022–1025.
38 D. Pradhan and I. N. Lin, *ACS Appl. Mater. Interfaces*, 2009, **1**, 1444.
39 S. A. Lyashenko, A. P. Volkov, R. R. Ismagilov and A. N. Obratsov, *Tech. Phys. Lett.*, 2009, **35**, 249–252.
40 K. Subramanian, W. P. Kang, J. L. Davidson, B. K. Choi and M. Howell, *Diamond Relat. Mater.*, 2006, **15**, 1994–1997.
41 O. Ivanov, V. Isaev, D. Radished, M. Lobaev, A. L. Visharev, V. Chernov, A. Kozlov and J. L. Hirshfield, *IEEE Trans. Plasma Sci.*, 2011, **39**(11), 2794–2795.
42 K. Y. Teng, H. C. Chen, H. Y. Chiang, C. C. Horng, H. F. Cheng, K. J. Sankaran, N. H. Tai, C. Y. Lee and I. N. Lin, *Diamond Relat. Mater.*, 2012, **24**, 126–133.
43 A. V. Karabutov, V. D. Frolov and V. I. Konov, *Diamond Relat. Mater.*, 2001, **10**, 840–846.
44 A. Wisitsora, W. P. Kang, J. L. Davidson and D. V. Kerns, *Appl. Phys. Lett.*, 1997, **71**(23), 3394–3396.
45 J. E. Butler and A. V. Sumant, *Chem. Vap. Deposition*, 2008, **14**, 146–160.
46 D. M. Gruen, *Annu. Rev. Mater. Sci.*, 1999, **29**, 211.
47 T. D. Corrigan, A. R. Krauss, D. M. Gruen, O. Auciello and R. P. H. Chang, *MRS Symposium Proc.*, 2000, **593**, 233.
48 D. M. Gruen, *MRS Bull.*, 2001, 771–776.
49 A. R. Krauss, O. Auciello, M. Q. Ding, D. M. Gruen, Y. Huang, V. V. Zhirnov, E. I. Givargizov, A. Breskin, R. Cheken, E. Shefer, V. Konov, S. Pimenov, A. Karabutov, A. Rakhimov and N. Suetin, *J. Appl. Phys.*, 2001, **89**, 2958.
50 V. D. Frolov, S. M. Pimenov, V. I. Konov, V. I. Polyakov, A. I. Rukovishnikov, N. M. Rossukanyl, J. A. Carlisle and D. M. Gruen, *Surf. Interface Anal.*, 2004, **36**, 449–454.
51 D. Zhou, A. R. Krauss, L. C. Qin, T. G. McCauley, D. M. Gruen, T. D. Corrigan, R. P. H. Chang and H. Gnaser, *J. Appl. Phys.*, 1997, **82**, 4546–4550.
52 T. D. Corrigan, D. M. Gruen, A. R. Krauss, P. Zapol and R. P. H. Chang, *Diamond Relat. Mater.*, 2002, **11**, 43–48.
53 J. Birrel, J. A. Carlisle, O. Auciello, D. M. Gruen and J. M. Gibson, *Appl. Phys. Lett.*, 2002, **81**, 2235–2237.
54 J. Birrel, J. E. Gerbi, O. Auciello, J. M. Bibson, D. M. Gruen and J. A. Carlisle, *J. Appl. Phys.*, 2003, **93**, 5606–5612.
55 R. Arenal, P. Bruno, D. J. Miller, M. Bleuel, J. Lai and D. M. Gruen, *Phys. Rev. B:Condens. Matter*, 2007, **75**, 195431.
56 K. Okano, S. Koizumi, S. R. P. Silva and G. A. J. Amaratunga, *Nature*, 1996, **381**, 140–141.
57 A. Ilie, A. C. Ferrari, T. Yagi, S. E. Rodil, J. Robertson, E. Barborini and P. Milani, *J. Appl. Phys.*, 2001, **90**(4), 2024–2032.
58 S. Orlanducci, A. Fiori, V. Sessa, E. Tamburri, F. Toschi and M. L. Terranova, *J. Nanosci. Nanotechnol.*, 2008, **8**, 3228–3234.
59 Y. C. Lin, K. J. Sankaran, Y. C. Chen, C. Y. Leee, H. C. Chen, I. N. Lin and N. H. Tai, *Diamond Relat. Mater.*, 2011, **20**, 191–195.
60 K. J. Sankaran, J. Kurian, H. C. Chen, C. L. Dong, C. Y. Lee, N. H. Tai and I. N. Lin, *J. Phys. D: Appl. Phys.*, 2012, **45**, 365303.
61 P. Deak, B. Aradi, M. Kaviani, T. Frauenheim and A. Gali, *Phys. Rev. B: Condens. Matter*, 2014, **89**, 075203.
62 V. P. Mammana, T. E. A. Santos, A. Mammana, V. Baranauskas, H. J. Ceragioli and A. C. Peterlevitz, *Appl. Phys. Lett.*, 2002, **81**, 3470.
63 V. Baranauskas, M. Fontana, H. J. Ceragiolo and A. C. Peterlevitz, *Nanotechnology*, 2004, **15**, S678–S683.
64 S. A. Lyashenko, A. P. Volkov, R. R. Ismagilov and A. N. Obratsov, *Tech. Phys. Lett.*, 2009, **35**, 249.
65 H. F. Cheng, K. Y. Teng, H. C. Chen, G. C. Tzeng, C. Y. Tang and I. N. Lin, *Surf. Coat. Technol.*, 2013, **228**, S175–S178.
66 A. Saravanan, B. R. Huang, K. J. Sankaran, C. L. Dong, N. H. Tai and I. N. Lin, *Appl. Phys. Lett.*, 2014, **104**, 181603.
67 V. V. Chernov, O. A. Ivanov, V. A. Isaev, D. B. Rasdishev, A. L. Visharev and A. V. Kozlov, *Diamond Relat. Mater.*, 2013, **37**, 87–91.
68 K. J. Sankaran, H. C. Chen, C. Y. Lee, N. H. Tai and I. N. Lin, *Appl. Phys. Lett.*, 2012, **101**, 241604.
69 K. J. Sankaran, H. C. Chen, B. Sundaravel, C. Y. Lee, N. H. Tai and I. N. Lin, *Appl. Phys. Lett.*, 2013, **102**, 061604.
70 K. J. Sankaran, K. Panda, B. Sundaravel and N. H. Tai, *J. Appl. Phys.*, 2014, **115**(6), 063701.
71 K. Panda, B. Sundaravel, B. K. Panigrahi, H. C. Chen, P. C. Huang, W. C. Shih, S. C. Lo, L. J. Lin, C. Y. Lee and I. N. Lin, *J. Appl. Phys.*, 2013, **113**, 094305.
72 K. J. Sankaran, H. C. Chen, K. Panda, B. Sundaravel, C.-Y. Lee, N.-H. Tai and I.-N. Lin, *ACS Appl. Mater. Interfaces*, 2014, **6**(7), 4911–4919.
73 A. S. Barnard, *Rev. Adv. Mater. Sci.*, 2004, **6**(94), 15.
74 S. B. Tian, Y. L. Li, X. X. Xia, C. Z. Gu and J. J. Li, *Phys. E.*, 2011, **43**, 1902.
75 C. E. Nebel, N. Yang, H. Uetsuka, E. Osawa, N. Tokuda and O. A. Williams, *Diamond Relat. Mater.*, 2009, **18**, 910–917.

76 X. Wang, L. E. Ocola, R. S. Divan and A. Sumant, *Nanotechnology*, 2012, **23**(7), 075301.
77 H. Masuda, T. Yanagishita, K. Yasui, K. Nishio, I. Yagi, T. N. Rao and A. Fijishima, *Adv. Mater.*, 2001, **13**, 247, 11.
78 M. Y. Chen, K. Y. Wu, J. Hwang, M. T. Chang, L. J. Chou and C. S. Kou, *Nanotechnology*, 2007, **18**, 455706.
79 S. Orlanducci, V. Guglielmotti, I. Cianchetta, V. Sessa, E. Tamburri, F. Toschi, M. L. Terranova and M. Rossi, *Nanosci. Nanotechnol. Lett.*, 2012, **4**, 338–343.
80 M. Sugawara, *Plasma Etching: Fundamentals and Applications*, Oxford University Press, New York, 1998.
81 *Handbook of Advanced Plasma Processing Techniques*, ed. R. J. Shul and S. J. Pearton, Springer, Berlin, NY, 2000.
82 K. Ostrikov, *Plasma Nanoscience*, Wiley-VCH, Weinheim, 2008.
83 *Plasma Processing of Nanomaterials*, ed. R. M. Sankaran, CRC Press, Boca Raton, 2011.
84 G. S. Sandhu and W. K. Chu, *Appl. Phys. Lett.*, 1989, **55**, 437.
85 B. R. Stoner, G. J. Tessmer and D. L. Dreifus, *Appl. Phys. Lett.*, 1993, **62**, 1803.
86 Y. Ando, Y. Nishibayashi and A. Sawabe, *Diamond Relat. Mater.*, 2004, **13**, 633.
87 W. Smirnov, A. Kriele, N. Yang and C. E. Nebel, *Diamond Relat. Mater.*, 2010, **19**, 186–189.
88 F. Weigl, S. Fricker, H.-G. Boyen, C. Dietrich, B. Kolowski, A. Plettl, O. Pursche, P. Zienann, P. Walther, C. Hartmann, M. Ott and M. Moeller, *Diamond Relat. Mater.*, 2006, **15**, 1689–1694.
89 J. Y. Lin, Z. C. Li, C. Y. Chen, L. J. Chou, J. C. Hwang and C. S. Kou, *Diamond Relat. Mater.*, 2011, **20**, 922–926.
90 S. Kunuku, K. J. Dankaran, C. Y. Tsai, W. H. Chang, N. H. Tai, K. C. Leou and I. N. Lin, *ACS Appl. Mater. Interfaces*, 2013, **5**(15), 7439–7449.
91 W. J. Zhang, X. Jiang and Y. B. Xia, *J. Appl. Phys.*, 1997, **82**, 1996.
92 Y. S. Zou, K. L. Ma, W. J. Zhang, Q. Ye, Z. Q. Yao, Y. M. Chong and S. T. Lee, *Diamond Relat. Mater.*, 2007, **16**, 1208.
93 Y. F. Tzeng, K. H. Liu, Y. C. Lee, S. J. Lin, I. N. Lin, C. Y. Lee and H. T. Chiu, *Nanotechnology*, 2007, **18**, 435703.
94 J. Y. Lin, S. H. Wang, T. T. Chen, C. Y. Chen, L. J. Chou, J. C. Hwang and C. S. Kou, *J. Electrochem. Soc.*, 2011, **158**, D426.
95 W. J. Zhang, Y. Wu, W. K. Wong, X. M. Meng, C. Y. Chan, I. Bello, Y. Lifshitz and S. T. Lee, *Appl. Phys. Lett.*, 2003, **83**, 3365.
96 W. J. Zhang, X. M. Meng, C. Y. Chan, Y. Wu, I. Bello and S. T. Lee, *Appl. Phys. Lett.*, 2003, **82**, 2622.
97 W. J. Zhang, Y. Wu, C. Y. Chan, W. K. Wong, X. M. Meng, I. Bello, Y. Lifshitz and S. T. Lee, *Diamond Relat. Mater.*, 2004, **13**, 1037–1043.
98 Q. Wang, Z. L. Wang, J. J. Li, Y. Huang, Y. L. Li, C. Z. Gu and Z. Cui, *Appl. Phys. Lett.*, 2006, **89**, 063105.
99 K. Panda, K. J. Sankaran, B. K. Panigrahi, N. H. Tai and I. N. Lin, *ACS Appl. Mater. Interfaces*, 2014, **6**(11), 8531–8541.
100 V. Chatterjee, R. Harniman, P. W. May and P. K. Barhai, *Appl. Phys. Lett.*, 2014, **104**, 171907.
101 Z. L. Wang, Q. Wang, H. J. Li, J. J. Li, P. Xu, Q. Luo, A. Z. Jin, H. F. Yang and C. Z. Gu, *Sci. Technol. Adv. Mater.*, 2005, **6**, 799–803.
102 Z. L. Wang, Q. Luo, J. J. Li, Q. Wang, P. Xu, Z. Cui and C. Z. Gu, *Diamond Relat. Mater.*, 2006, **15**, 631–634.
103 K. J. Sankaran, N. H. Tai and I. N. LiN, *Appl. Phys. Lett.*, 2014, **104**, 031601.
104 V. N. Mochalin, O. Shenderova, D. Ho and Y. Gogotsi, *Nat. Nanotechnol.*, 2012, **7**(1), 11–23.
105 A. I. Lymkin, E. A. Petrov, A. P. Ershov, G. V. Sakovitch, A. M. Stayer and V. M. Titov, *Dokl. Akad. Nauk. USSR*, 1988, **302**, 611–613.
106 N. R. Greiner, D. S. Philips, J. D. Johnson and F. Volk, *Nature*, 1988, **333**, 440–442.
107 V. V. Zhirnov, O. A. Shenderova, D. L. Jaeger, A. Tyler, A. A. Areskin, D. W. Brenner and J. J. Hren, *Phys. Solid State*, 2004, **46**, 657–651.
108 A. S. Barnard and M. Sternberg, *J. Mater. Chem.*, 2007, **17**, 4811–4819.
109 J. Y. Raty and G. Galli, *Nat. Mater.*, 2003, **2**(12), 792–795.
110 O. Shenderova and G. McGuire, *Handbook of Nanomaterials*, ed. Yu Gogotsi, CRC Press, Boca Raton, 2006, p. 201.
111 M. Baidakova and A. A. Y. Vul', *J. Phys. D: Appl. Phys.*, 2007, **40**, 6300.
112 O. A. Shenderova and D. M. Gruen, *Nanocrystalline Diamond: synthesis, properties and applications*, Google e-book, 2012.
113 *Detonation Nanodiamonds: Fabrication, Properties and Applications. Proc 1st Int. Symp.*, St. Petersburg, 2003.
114 D. M. Gruen, O. Shenderova and A. Y. Vul', *Synthesis, Properties and Applications of Ultrananocrystalline Diamond*, Springer, 2005, vol. 192.
115 A. Aleksenskiy, M. Baidakova, V. Osipov and A. Y. Vul', *The Fundamental Properties and Characteristics of Nanodiamonds in "Nanodiamonds"*, ed. D. Ho, Springer, 2010, pp. 55–77.
116 S. H. Hsu, W. P. Kang, J. L. Davidson, J. H. Huang and D. V. Kerns, *J. Appl. Phys.*, 2012, **111**, 114502.
117 S. H. Hsu, W. P. Kang, J. L. Davidson and J. H. Huang, *IEEE Trans. Electron Devices*, 2013, **60**, 487–493.
118 N. Heidrich, J. Hees, V. Zuerbig, D. Iankov, W. Pletdchen, R. H. Dah, B. Rasynor, L. Kirste, C. E. Nebel, O. Ambacher and V. Lebedev, *Transducers Eurosens.*, 2013, 218–221.
119 C. M. Posada, E. J. Grant, R. Divan, A. V. Sumant, D. Rosenmann, L. Start, H. K. Lee and C. H. Castano, *J. Appl. Phys.*, 2014, **115**(13), 134506.
120 W. P. Kang, J. L. Davidson, A. Wisitsora, M. Howell, A. Jamaludin, Y. M. Wong, K. L. Soh and D. V. Kerns, *J. Vac. Sci. Technol., B*, 2003, **21**, 192–195.
121 K. Subramanian, W. P. Kang, J. L. Davidson and W. H. Hofmeister, *Diamond Relat. Mater.*, 2005, **14**, 404–410.
122 K. Subramanian, W. P. Kang, J. L. Davidson, W. H. Hofmeister, B. K. Choi and M. Howell, *Diamond Relat. Mater.*, 2005, **14**, 2099–2104.

123 K. Subramanian, W. P. Kang, J. L. Davidson, N. Gosh and K. F. Galloway, *Microelectron. Eng.*, 2011, **88**, 2924–2929.
124 W. P. Kang, S. H. Hsu, N. Ghosh, J. L. Davidson, J. H. Huang and D. V. Kerns, *25th IVNC- International Vacuum Nanoelectronic Conference*, 2012, pp. 1–2, DOI: 10.1109/IVNC.2012.6316869.
125 W. Prost, U. Auer, F. J. Tegude, C. Pacha, K. F. Goser, G. Janssen and T. van der Roer, *Int. J. Circuit Theory Appl.*, 2000, **28**, 537–552.
126 N. Ghosh, W. P. Kang and J. L. Davidson, *Diamond Relat. Mater.*, 2012, **23**, 120–124.
127 X. Li, M. Li, L. Dan, Y. Liu and C. Tang, *Phys. Rev ST Accel. Beams*, 2013, **16**, 123401.
128 N. Yang, H. Uetsuka, O. A. Williams, E. Osawa, N. Tokuda and C. E. Nebel, *Phys. Status Solidi A*, 2009, **206**(9), 2048–2056.
129 C. Lu, Y. Li, S. Tian, W. Li and C. Gu, *Microelectron. Eng.*, 2011, **88**(8), 2319–2321.
130 B. J. M. Hausmann, M. Kahn, Y. Zhang, T. M. Babinec, K. Martinick, M. McCutcheon, P. R. Emmer and M. Loncar, *Diamond Relat. Mater.*, 2010, **19**(5–6), 621–629.

